

**ESTIMATING TERRESTRIAL CARBON SEQUESTERED IN ABOVEGROUND  
WOODY BIOMASS FROM REMOTELY SENSED DATA**

*(The use of SEBAL and CASA algorithms in a semi-arid area of  
Serowe-Botswana)*

**Lemmy Nenge Namayanga  
March 2002.**

**ESTIMATING TERRESTRIAL CARBON SEQUESTERED IN ABOVEGROUND  
WOODY BIOMASS FROM REMOTELY SENSED DATA.**

*(The use of SEBAL and CASA algorithms in a semi-arid area of Serowe-Botswana)*

**By:**  
**Lemmy Nenge Namayanga**  
**March 2002**

**Authoritative Statement:**

This thesis submitted in partial fulfilment of the requirements for the award of a *Master of Science Degree in Environmental Systems Analysis and Management* – International Institute for Geo-Information Science and Earth Observation (ITC), Enschede-The Netherlands.

**Examination Board:**

**Co-supervisor:** *Prof. Alfred de Gier.*

**Supervisor:** *Dr. Iris van Duren.*

**External Examiner:** *Mr. Dennis Rugege (University of KwaZulu Natal, South Africa).*



**INTERNATIONAL INSTITUTE FOR GEO-INFORMATION SCIENCE AND EARTH  
OBSERVATION  
ENSCHEDÉ, THE NETHERLANDS**

## Disclaimer

*This document describes work undertaken as part of a programme of study at the International Institute for Geo-Information Science and Earth Observation. All views and opinions expressed therein remain the sole responsibility of the author, and do not necessarily represent those of the institute.*

*“Assimilation of carbon dioxide is the sine qua non of competitive success in green plants. All other aspects of physiological functioning are ancillary to it. Even the production of seed may be thought of as a strategy to establish new centres of carbon fixation and, in that general sense, the associated metabolic cost is no different in kind from that expended, say, by a tree in maintaining its foliage in the sun.” (Cowan, 1978) from Lange et al., 1982.*

## ABSTRACT

Lack of cheaper, precise, universally applicable, and environmentally benign approaches in the quantification of carbon sequestered in aboveground woody biomass has contributed to the controversial ratification and slow implementation of the Kyoto Protocol. However, the drafting of the Kyoto Protocol has made the subject of carbon sequestration become stronger and more important. Many researchers have shown that dry matter (biomass) is a time-integrated product of fractional photosynthetically active radiation ( $fPAR$ ) and incoming solar radiation ( $K_d$ ). This research study explored the use of remote sensing and GIS in the estimation of carbon sequestered in a semi-arid area through the use of the Surface Energy Balance Algorithm for Land (*SEBAL*) and the Carnegie Ames, Stanford Approach (*CASA*). Having allometrically estimated the aboveground woody biomass in-situ and consequently the amount of carbon sequestered in  $t/ha$ , remotely sensed data was used to estimate the amount of carbon sequestered over the same area. Field estimations of fresh weight aboveground woody biomass in Serowe-Botswana gave an average biomass stock of  $13 \pm 3 t/ha$  translating to  $3.9 \pm 0.5 tC/ha$  over the entire study area. Carbon stock values ranged from 52 tC/ha in the sandveld stratum to 150 tC/ha in the escarpment woodland. The *SEBAL-CASA* remote sensing approach yielded a negative value of  $11 \pm 0.7 t/ha$  convertible to a negative value of  $5 \pm 0.3 tC/ha$ . The estimated difference for the two approaches thence gave a value of 8.93 suggesting the acceptance of the alternate hypothesis. However, trends of the estimates of these methods correlate well. The high difference suggested by the statistics could be interpreted as the uncertainties associated with the use of limited meteorological data in the remote sensing approach. A carbon conversion factor specifically generated for the study area by means of laboratory analysis was found to be 0.43 and comparable to the factors of 0.46 and 0.5. Although the results in this study show a significant difference between the two methods, the remote sensing approach shows potential to accurately estimate carbon. Relationships between water, carbon and energy have been explored and gave an insight in the possible application of remote sensing in carbon monitoring and management projects when carbon becomes an internationally tradable commodity.

## ACKNOWLEDGEMENTS

In the first instance, my heart felt gratitude go to the *Dutch Government* and my employer-the *Environmental Council of Zambia (ECZ)* for having accorded me the opportunity to pursue my *MSc.* studies at the International Institute for Geo-Information Science and Earth Observation (*ITC*). In the same manner, I acknowledge the courtesy of the *SAFARI 2000* project for the free provision of the LandSat-7 ETM+ satellite images of the study area and the *Geological Survey Department (GS) of the Government of Botswana* for the hospitality, transport and camping gear provided and enjoyed during fieldwork. Many thanks too go to *Brand Wessels* of the *Forestry and Forest Products Research Centre (CSIR) of South Africa* for the Chemical analysis of the wood samples.

Special thanks to my Supervisors *Dr. Iris van Duren* and *Prof. Alfred de Gier* for their invaluable guidance, positive criticisms and technical support both in the field and at *ITC* during the construction of this thesis. Taking part too in this cake sharing are Messer's Gabriel Parodi and Wim Timmermans for their guidance on the *SEBAL* studies.

To the Jamaicans, *Jenevy Smith* and *Kirk Freckleton*, many many thanks for the support, encouragement and invaluable friendship you accorded to me. Hey! The six flags was an experience na half. Kirk! I'll remember you for the statement you made after your first trip to mother Africa "Mr. Lemmy, there is no excuse for such underdevelopment." To *Gwendoline Seke*, my gratitude for letting me use thy computer, for thy friendship and encouragement. To *Allan David Mulando*, thanks man for the ArcInfor segment closing tricks.

Finally but not definitely the least, I would also like to thank my fellow students for the warm and homely atmosphere we created in the process of beating nostalgia. Particular special thanks go to *Andres Hernandez Riguene* for being such a terrific counterpart in the field. Spicing it up were *Alejandra Fregoso*, *Liliosa Magombedze*, *Diana Chilvaro* and *Madana Priya*. Memories of *ITC* shall never be complete without remembering the *ACE Division MSc.* Students, Staff and colleagues. Hey! Guys, you have been good friends. I hope our parting would not mean the end of our friendship. To the Botswana camping crew, me say "tswee tswee, keep on being a good lot."

## DEDICATION

To Clara Kosamu Namayanga and daughter Inonge Bertha Namayanga for their patience, encouragement, understanding and resilience while I was away from them.

## TABLE OF CONTENTS

<b>1. INTRODUCTION</b> .....	<b>1</b>
<b>1.1. Background</b> .....	<b>1</b>
1.1.1. Carbon Sequestration: Why and what is it? .....	1
1.1.2. Sequestration in Semi-arid Environments.....	2
1.1.3. Carbon Allocation in Woody Plants (Trees and Shrubs).....	2
1.1.4. Biomass/Carbon Measurement Methods .....	3
<b>1.2. Field Methods for Biomass Estimation</b> .....	<b>4</b>
<b>1.3. Remote Sensing Methods for Biomass Estimation</b> .....	<b>4</b>
1.3.1. Use of Reflection Coefficients .....	4
1.3.2. Use of Solar radiation .....	4
<b>1.4. Research Justification</b> .....	<b>5</b>
1.4.1. Research Objectives and Purposes.....	5
1.4.2. Research Questions .....	6
<b>1.5. Hypotheses</b> .....	<b>6</b>
1.5.1. Field and Remotely Sensed Measurements .....	6
1.5.2. Is Carbon Content Species Dependent? .....	6
<b>2. THEORY AND PRACTICE OF THE ENERGY BALANCE EQUATION</b> .....	<b>7</b>
<b>2.1. The Energy Balance Equation</b> .....	<b>7</b>
2.1.1. Energy and Biomass.....	7
2.1.2. The CASA Overview .....	8
2.1.3. The SEBAL Overview .....	8
2.1.4. Energy Balance Equation-Relationships Between Carbon and Water .....	9
2.1.5. The Evaporative Fraction.....	10
2.1.6. Other Key Variables for Energy Balance Equations .....	11
<b>2.2. Biomass Calculation from SEBAL and CASA algorithms.</b> .....	<b>12</b>
<b>2.3. The difference between Production and Productivity</b> .....	<b>13</b>
<b>3. DESCRIPTION OF THE STUDY AREA</b> .....	<b>14</b>
<b>3.1. Location</b> .....	<b>14</b>
<b>3.2. Climate</b> .....	<b>14</b>
<b>3.3. Vegetation</b> .....	<b>15</b>
<b>3.4. Coal Mining and Power Generation</b> .....	<b>16</b>
<b>4. METHODS AND MATERIALS</b> .....	<b>17</b>
<b>4.1. Pre-fieldwork</b> .....	<b>17</b>
4.1.1. Sampling Design .....	17
4.1.2. Allometric Biomass Equations.....	18
<b>4.2. Fieldwork</b> .....	<b>18</b>
4.2.1. Tree Cover, Species and Height.....	19
4.2.2. Meteorological Measurements.....	19
<b>4.3. Post fieldwork Activities</b> .....	<b>20</b>

4.3.1.	Tree Cover (%).....	20
<b>4.4.</b>	<b>Field Biomass Estimations of Aboveground Woody Vegetation .....</b>	<b>20</b>
4.4.1.	The Dumas-Method- Laboratory Analysis for Carbon Content .....	21
4.4.2.	Biomass and Carbon Estimation from Remotely Sensed Data.....	22
<b>4.5.</b>	<b>Field Biomass and Remotely-Sensed Biomass.....</b>	<b>22</b>
4.5.1.	Assumptions.....	23
<b>5.</b>	<b>RESULTS .....</b>	<b>24</b>
<b>5.1.</b>	<b>General.....</b>	<b>24</b>
5.1.1.	Tree Cover (%).....	24
5.1.2.	NDVI as an Indicator of Biomass .....	24
5.1.3.	Meteorological Results .....	25
<b>5.2.</b>	<b>Field Biomass Estimation of Aboveground Woody Vegetation.....</b>	<b>26</b>
<b>5.3.</b>	<b>Tree Cover, NDVI and Fresh Biomass Relationships .....</b>	<b>27</b>
<b>5.4.</b>	<b>Determined Carbon Content in Serowe Species.....</b>	<b>29</b>
5.4.1.	Dry weight biomass and Carbon content .....	30
5.4.2.	Comparison of carbon content factors .....	30
<b>5.5.</b>	<b>The Vegetation and Carbon Maps .....</b>	<b>30</b>
<b>5.6.</b>	<b>Biomass Estimation from Remote Sensing .....</b>	<b>31</b>
5.6.1.	Biomass/Carbon Estimates from Remote Sensing.....	32
<b>5.7.</b>	<b>Comparison of the Estimates from the Two Methods.....</b>	<b>33</b>
<b>5.8.</b>	<b>The Carbon Status in Serowe .....</b>	<b>34</b>
<b>6.</b>	<b>DISCUSSION.....</b>	<b>35</b>
<b>6.1.</b>	<b>Vegetation and the Serowe Environment. ....</b>	<b>35</b>
6.1.1.	Tree Cover and Biomass .....	36
6.1.2.	NDVI as a Biomass Predictor .....	36
<b>6.2.</b>	<b>Field/Remote Measurements of Biomass .....</b>	<b>37</b>
<b>6.3.</b>	<b>The Serowe Carbon Conversion Factor.....</b>	<b>38</b>
<b>6.4.</b>	<b>Comparisons Between Field and Remote Measurements .....</b>	<b>39</b>
<b>7.</b>	<b>CONCLUSIONS &amp; RECOMMENDATIONS.....</b>	<b>40</b>
<b>7.1.</b>	<b>Study Outputs.....</b>	<b>40</b>
7.1.1.	Conclusions.....	40
7.1.2.	Recommendations.....	40
<b>7.2.</b>	<b>Application of Research.....</b>	<b>40</b>
	<i>REFERENCES:</i> .....	42
	<i>APPENDICES:</i> .....	45

## LIST OF FIGURES

Figure 3.1: <i>The relative position of the study area</i> .....	16
Figure 3.1: <i>Daily measurements of temperature and wind speed respectively from 10/01/86 to 01/01/94. Note data gaps in the wind speed graph</i> .....	17
Figure 3.1: <i>Escarpment (left) and hardveld (right) vegetation. September 18, 2001</i> .....	18
Figure 4.1: <i>Field biomass/carbon flowchart</i> .....	23
Figure 4.2: <i>Sequential steps in the determination of carbon from remotely sensed data</i> ....	24
Figure 4.3: <i>Theoretical construction of the comparison and validation summary of the procedure</i> .....	25
Figure 5.1: <i>Tree cover (%) frequency per cover class</i> .....	26
Figure 5.2: <i>NDVI (bands 3 &amp; 4) combinations from Landsat-7 ETM+ of August 11, 2000</i> .....	27
Figure 5.3: <i>(left to right, top)-air temperature and incoming solar radiation; (left to right, bottom)-relative humidity and soil temperature</i> .....	27
Figure 5.4: <i>Total fresh weight biomass per sample plot with and without the outlier in plot 65 respectively</i> .....	28
Figure 5.5: <i>Frequency of total fresh weight biomass</i> .....	28
Figure 5.6: <i>Total fresh weight biomass per stratum</i> .....	29
Figure 5.7: <i>Total aboveground fresh weight biomasses of each stratum as explained by tree cover and NDVI</i> .....	30
Figure 5.8: <i>Summaries of the relationships between total aboveground fresh weight biomass and total tree cover and NDVI for all the sampling plots</i> .....	30
Figure 5.9: <i>Mean oven-dry carbon content per species; n = 5</i> .....	31
Figure 5.10: <i>Carbon sequestered totals per stratum</i> .....	32
Figure 5.11: <i>A vegetation map of Serowe</i> .....	33
Figure 5.12: <i>A carbon map for Serowe</i> .....	33
Figure 5.13: <i>APAR (W/m<sup>2</sup>) map over the study area</i> .....	33
Figure 5.14: <i>Relationship between FPAR as a function of NDVI</i> .....	34
Figure 5.15: <i>Remote biomass estimates as explained by field oven-dry total biomass</i> .....	34
Figure 5.16: <i>Carbon sequestration estimates (t/ha) from remote sensing</i> .....	36

## LIST OF TABLES

Table 2.1: <i>Other key EBE variables</i> .....	13
Table 4.1: <i>ADAS measured parameters</i> .....	22
Table 5.1: <i>Tree height statistics for the study area</i> .....	26
Table 5.2: <i>Physical height of the vegetation per stratum</i> .....	26
Table 5.3: <i>Stratified random sampling results for aboveground woody fresh weight biomasses</i> .....	29
Table 5.4: <i>ANOVA of carbon content (%) in oven dry branch samples of tree and shrub species; P = 0.05; N = 50</i> .....	31
Table 5.5: <i>Mean carbon content variance, P = 0.05</i> .....	32
Table 5.6: <i>Stratum biomass and carbon amounts comparisons</i> .....	32
Table 5.7: <i>Field carbon estimates versus remote carbon estimates</i> .....	35
Table 5.8: <i>The regression analysis of remotely sensed and field measured carbon values</i> ..	35
Table 5.9: <i>Statistics of sequestered carbon in Serowe</i> .....	35
Table 5.10: <i>summary of the carbon status (baseline distribution) in Serowe</i> .....	35

## LIST OF ACRONYMS USED IN THE THESIS

<b>ADAS</b>	Automatic Data Acquisition System
<b>APAR</b>	Absorbed Photosynthetically Active Radiation
<b>C</b>	Carbon
<b>CASA</b>	Carnegie, Ames, Stanford Approach
<b>CDMs</b>	Clean Development Mechanisms
<b>C/N</b>	Carbon Nitrogen Ratio
<b>DBH</b>	Diameter at Breast Height
<b>DOE</b>	Department of Energy of the United States of America
<b>EBE</b>	Energy Balance Equation
<b>EET</b>	Estimated actual Evapotranspiration
<b>EMS</b>	Electromagnetic Spectrum
<b>FAO</b>	World Food and Agriculture Organisation
<b>FETC</b>	Federal Energy Technology Centre
<b>FCCC</b>	Framework Convention on Climate Change
<b>FDBR</b>	Fresh-Dry weight Biomass Ratio (0.5505)
<b>FPAR</b>	Fractional Photosynthetically Active Radiation
<b>GCMs</b>	Global Climate Models
<b>GHE</b>	Greenhouse Effect
<b>GHGs</b>	Greenhouse Gases
<b>GIS</b>	Geographical Information System
<b>GPP</b>	Gross Primary Production
<b>GPS</b>	Global Positioning System
<b>Gt</b>	Giga-tonnes (10 <sup>9</sup> )
<b>ILWIS</b>	Integrated Land and Water Information System
<b>IPCC</b>	International Panel on Climate Change
<b>ISLSCP</b>	International Satellite Land Surface Climatology Project
<b>ITC</b>	International Institute for Geo-Information Science and Earth Observation
<b>JI</b>	Joint Implementation
<b>LAI</b>	Leaf Area Index
<b>LandSat</b>	Land Survey Resource Satellite Programme.
<b>NASA</b>	National Aeronautics and Space Administration
<b>NDVI</b>	Normalized Difference Vegetation Index
<b>NIR</b>	Near-Infra-Red
<b>NPP</b>	Net Primary Production
<b>NTSG</b>	Numerical Terradynamic Simulation Group
<b>PAR</b>	Photosynthetically Active Radiation
<b>PET</b>	Potential Evapotranspiration
<b>SAFARI-2000</b>	Southern African Regional Science Initiative
<b>SEBAL</b>	Surface Energy Balance Algorithm for Land
<b>TROFs</b>	Tree Resources Outside Forests
<b>Umich</b>	University of Michigan-USA
<b>UNEP</b>	United Nations Environment Programme
<b>UNFCCC</b>	United Nations Framework Convention on Climate Change
<b>UTM</b>	Universal Transverse Mercator
<b>VNIR</b>	Visible, Near-Infra-Red
<b>VPD</b>	Vapour Pressure Deficit

## 1. INTRODUCTION

### 1.1. Background

In 1896, a Swedish chemist, Svante Arrhenius (NASA, 2001) made a prediction of climate change due to human activities. Over, 100 years now after this prediction, the world is aware that carbon dioxide ( $CO_2$ ) emissions particularly those from fossil fuel burning are increasing and causing global warming. As (NASA, 2001) observes, these emissions are likely to double by the middle of the next century from levels at Arrhenius' time. This coupled with evidences of global warming put forth by the Working Groups' of the Framework Convention on Climate Change (FCCC)'s technical reports, compelled the world to respond by the drafting of the Kyoto Protocol (UNFCCC, 1997).

With the drafting of the Kyoto Protocol, the subject of carbon sequestration has become stronger and important. The Protocol represents an international effort in limiting the continued release of greenhouse gases (GHGs) into the atmosphere by 5% lower than 1990 levels by 2012 and mitigate global warming. To expedite and achieve this, the Kyoto Protocol has attempted to motivate the world by adding an economic value to the management of carbon. However, the implementation of this protocol has met a number of challenges. One of these is the lack of an agreed upon method to be used in the quantification and monitoring of carbon sequestration. When carbon becomes an internationally tradable commodity, accurate, precise, environmentally benign and cost effective methods will inevitably be required.

The mitigation of global warming is faced with controversies mainly due to the fact that the atmosphere is a complex entity to deal with and that it is an example of the adage 'tragedy of the commons'. However, terrestrial carbon sequestration in above ground woody biomass has received attention as a promising course in an immediate attempt to mitigate global warming. Although many types of carbon sequestration have been identified, this study focuses on terrestrial sequestration in aboveground woody biomass. This is so because photosynthesis is the major natural direct way by which  $CO_2$  in the atmosphere is fixed back to earth and that satellite sensors effectively record characteristics of the biosphere occurring at the Earth's surface.

Biomass density estimates provide the means for estimating the amount of carbon sequestered on a given area over time (Brown, 1997) with the amount of carbon being calculated as a fraction of the oven-dry weight biomass. (FAO, 2001) reports that an estimated 125 gigatonnes (*Gt*) of carbon are exchanged annually between vegetation, soils and the atmosphere, with terrestrial sequestration accounting for two-fifths of the total exchange. Conventionally, biomass estimation in forests requires cutting, which contributes to the reduction of the carbon sink pool size. Hence, estimating carbon from remotely sensed data may contribute positively to the mitigation of global warming. However, the ways and means of doing this are currently underdevelopment. Nonetheless, many of the relationships between the needed parameters are already available making the complex task relatively easier. Thus, the essence of this exploratory study is to attempt to employ remote sensing approaches in estimating carbon sequestered in aboveground woody biomass.

#### 1.1.1. Carbon Sequestration: Why and what is it?

Carbon sequestration is the capture and secure storage of carbon that would otherwise be wantonly emitted to or remain in the atmosphere and enhance the greenhouse effect process

(Houghton, 1996). (DOE, 2001) explicitly defines terrestrial carbon sequestration distinguishing it from other carbon sequestration potentials. Terrestrial ecosystems store substantial amounts of fixed cellulose and lignin in a more readily utilisable form (wood). (Brown, 1997) reports that biomass of forests provides estimates of carbon pools because about 50% of the pools is carbon. Wood whose main constituent is carbon also acts as a storage reservoir for water, nutrients and carbohydrates (Lange O. L. et al., 1982). The process of wood formation therefore, improves the carbon balance with respect to respiratory  $CO_2$  loss when compared with herbaceous (mostly grasses and forbs) plants on a relative scale.

TROFs (Tree Resources Outside Forests) may also undoubtedly and significantly contribute to the net  $CO_2$  reduction in the atmosphere if promoted and help check global warming. Apart from sequestering carbon, increasing terrestrial carbon pool sizes also provides additional benefits such as these:

- stabilising the hydrological cycle and improving land characteristics such as soil organic matter from increased afforestation,
- slowing or stopping the loss of existing forests, thus preserving current carbon reservoirs (WRI, 2001),
- enhancing landscape sceneries-adding to the planet's vegetative cover through reforestation thus enlarging living terrestrial carbon reserves,
- increasing the carbon stored in artificial reserves, including timber products (WRI, 2001)
- improving air quality and micro environments, and
- provision of employment thereby improving the livelihoods of many people especially in rural areas.

### **1.1.2. Sequestration in Semi-arid Environments**

According to literature (IPCC, 2000), soils' capabilities to sequester carbon seem to be larger than the aboveground woody pool but this largely depends on spatial location and vegetation availability. The carbon-nitrogen ( $C/N$ ) ratio of soil organic matter depends on the  $C/N$  ratio of the vegetational inputs and the degree to which they are composed (Sumner, 2000) Tropical and semi-arid soils are reportedly said to store very little carbon in form of soil organic matter as compared to temperate grasslands, due to high temperatures (Sumner, 2000). On the other hand the (IPCC, 2000) shows that soils sequester more carbon than the vegetation.

Sandy (arenosols) soils, the type of soil prevalent in the study area of Serowe-Botswana are naturally supposed to be well aerated thus being high oxidising environments enhancing the rate of decomposition and leaching. Grasses sequester substantial amounts of carbon mainly on a seasonal basis like crops but they are a temporal store of carbon especially in the tropics and semi-arid environments where this is further worsened by frequent rampant bush fires. In regard of the above, this inadvertently leaves trees as a relatively short-term credible sink of  $CO_2$  and the centre of this research.

### **1.1.3. Carbon Allocation in Woody Plants (Trees and Shrubs)**

According to (Moll and Moll, 1994) wood is comprised of four basic materials namely: cellulose accounting for 50% or more of the bulk; hemi-cellulose-20%; lignin-25% and resin or oils accounting for the remainder. (Brown, 1997), reports that carbon quantities are about 50% of the aboveground woody biomass weight. Woody plants are characterized by

secondary growth and a continuous conversion of structural tissue into non-living, therefore non-respiring biomass. This leads to the increase in girth of a plant due to the lateral meristem action of the vascular cambium producing the secondary xylem popularly known as wood. This dry matter remains an integral part of an individual tree essential to its functioning. As (Costa, 1996) writes, plant tissues vary in their carbon storage with stems and fruits having more carbon per gram of dry weight than leaves and that longer-lived trees with high-density wood store more carbon per volume than short-lived, low-density, fast-growing ones.

The above paragraph provides a good biological fact-sheet against people who argue that terrestrial carbon sequestration is temporal and thence should not be advocated. Isn't it true that every thing in nature is in a state of flux? It all depends on the recycling rate or time scale. It may be argued that in carbon sequestration, it is not the absolute volume of carbon uptake but rather the change in the rate of carbon storage versus release over time. Until that rate is reduced or reversed, carbon build-up in the atmosphere will continue, as fate would have it.

#### 1.1.4. Biomass/Carbon Measurement Methods

In line with the Kyoto Protocol, many researchers have developed various methods for the quantification of sequestered carbon. However, many of these methods are very complicated, expensive and limited in their spatial coverage. Such limitations impede the sound quantification and monitoring of carbon. Remote sensing may thus provide an answer against such measurement and monitoring limitations. The remote sensing approach can meet the requirements of carbon sequestration such as permanent sample plots (MacDicken, 1997) achieved by means of fixed coordinates coupled with the systematic repetitive characteristic of most satellites; the economic realities of costs and benefits and the environmentally benignness that the technique provides. (Tucker, 1979); (Richardson et al., 1983); and (Christensen and Goudriaan, 1993), demonstrated that the reflection of the red, green and near-infrared (*NIR*) radiation contains considerable information about plant biomass. However, they further found that the reflection coefficients determined are not stable because they do not represent the amount of dry matter but that of green foliage biomass that is phenologically affected.

Thus, the other approach based on the positively determined relationship between the amount of dry matter and accumulated intercepted photosynthetically active radiation ( $4 - 7 \mu m$ ) (Monteith, 1977 in (Christensen and Goudriaan, 1993) was explored. Many researchers have shown that dry matter is a time-integral product of fractional photosynthetically active radiation (*FPAR*) and daily incident short-wave radiation ( $K\downarrow$ ). Considering the fact that parameters such as  $K\downarrow$ , *NDVI*, air temperature (*T<sub>a</sub>*), wind speed (*u*) and moisture may vary from pixel to pixel (land parcel to land parcel), an algorithm that takes into consideration the instantaneous variation of these parameters with respect to the expanse of land was sought.

The Surface Energy Balance Algorithm for Land (*SEBAL*) was adopted. *SEBAL* calculates an evaporative fraction (*A*) that is used as an input in the Carnegie-Ames-Stanford Approach (*CASA*) model to yield biomass. As (Goward et al., 1985) reports "the flux of latent heat ( $\lambda E$ ) associated with evaporative losses has been shown by numerous authors to be the dominant energy exchange process in vegetated landscapes".  $K\downarrow$  provides the energy for photosynthesis, transpiration and evaporation and thus balancing and studying it with respect to land characteristics provides a good estimate of the energy exchanges with the atmosphere.

## 1.2. Field Methods for Biomass Estimation

There is a greater choice of available methods for field biomass estimations. (Brown, 1997) stipulates that more often than not these methods apply to closed forests, open forests, woodlands, woody savannahs, woodlots, line tree plantings, home gardens, living fences and many more cover groupings. To estimate total organic carbon, a substantial proportion of biomass, requires a complete enumeration of the entire ecosystem's components that may include saplings, vines, epiphytes, and dead plant matter such as standing woody stems. To account for all these in one method makes the method not only difficult and lengthy but also tedious and expensive.

Therefore, for practical reasons, this study restricted itself to the aboveground woody living component of biomass from which total carbon stored was determined. (Tietema, 1993)'s allometric equations were used herein to estimate the aboveground fresh weight biomass. See chapter 4 for details.

## 1.3. Remote Sensing Methods for Biomass Estimation

(Christensen and Goudriaan, 1993) demonstrated that reflections of the red, green and near infrared radiances contained considerable information about crop biomass owing to the contrasts between soil and vegetation. (Sellers, 1987) also reports that many researchers have utilised combinations of spectral radiances over vegetated surfaces as indicators of density, health or biomass of the vegetation. Thus, many vegetation indices today exist of which the most common and simple ones are: the relative vegetation index (*RVI*), and the normalised difference vegetation index (*NDVI*). See appendix BII more indices and details).

Therefore, for the purposes of predicting biomass from spectral reflection indices as reported in Christensen and Goudriaan (1993), two main approaches have been followed:

### 1.3.1. Use of Reflection Coefficients

The use of correlations between *RVI* or *NDVI* and biomass ((Tucker, 1979); (Richardson et al., 1983); (Tucker et al., 1983); and Ahlrichs and Baner, 1983 and Petersen, 1989 in (Christensen and Goudriaan, 1993) has been found to be unstable. This is because the reflection coefficients are primarily determined by green foliage biomass and not the amount of dry matter (Christensen and Goudriaan, 1993). They further elucidate that during the growth of a plant, accumulated dry matter increases relatively more than the current green foliage does. Thence, considering this led to a second approach that is based on the relationship between the amounts of dry matter and accumulated intercepted photosynthetically active radiation.

### 1.3.2. Use of Solar radiation

Solar radiation available for photosynthesis (known as photosynthetically active radiation-*PAR*) has been known to regulate ecological production for a long time. Literature suggests that this relationship was first modelled by Monteith in 1977 while experimental results (citations in Christensen and Goudriaan, 1993) have shown that dry matter (biomass) is a time-integrated product of '*fPAR*' and '*K<sub>d</sub>*' as explained in section 1.1.4. Although this approach is widely known among ecologists, it has rarely been applied and tested in natural ecosystems. If applied, it has usually been done in hydrological studies. In this study attempts

to employ this approach for the purposes of estimating carbon from remotely sensed data are the subject. However, doing this demands the combination of *SEBAL* and *CASA* algorithms as explained in chapter 2.

#### **1.4. Research Justification**

As the problem of  $CO_2$  emissions continues, part of the mitigation efforts rely in the development and availability of accurate, precise, environmentally benign and cost-effective methods for measuring the quantity of carbon sequestered. Although conventional methods for the estimation of biomass may be very accurate, their usage in carbon sequestration quantification is limited by some of the reasons given above. Therefore, remote sensing and GIS approaches may offer a better alternative in this regard. As (Sellers et al., 1995) and (Bastiaanssen et al., 1998) report, some methods in biomass/carbon estimation in plants using remote sensing have been developed but very little validation of the land surface prognostic or diagnostic variables have generally been attempted. In this study an attempt is made to use and validate such an approach.

In line with the quantification of carbon, (Davis et al., 2000) identified three broad categories in which current studies of Earth-Atmosphere  $CO_2$  fluxes can be divided. The first approach is the use of temporal and spatial patterns of  $CO_2$  concentrations to infer surface-atmosphere fluxes. Inversion models are examples. Approach two is observing fluxes directly with measurements of tower-based eddy covariance; excellent for local examinations but extrapolating the result over large regions is problematic. Approach three in which this study falls is the observation of earth's biomass to infer biosphere-atmosphere carbon exchange.

(Frouin and Pinker, 1995) report that primary productivity is regulated by photosynthetically active radiation (*PAR*), which is part of the electromagnetic spectrum (*EMS*) that consists of energy carrying photons. Part of this energy is what remote sensors record. (Umich, 2001) and (Dingman, 1994) allude to the fact that energy is used up and lost as heat as it flows through an ecosystem while new energy is continually being added to the earth in the form of solar radiation. In this regard, with respect to energy, the earth is considered as an open system. Therefore, dealing with energy in an instantaneous manner may be regarded as a best way to consider in carbon estimations from remote sensing. Hence, the use of the *SEBAL* and *CASA* algorithms is justified for the purpose of this study.

##### **1.4.1. Research Objectives and Purposes.**

Remote sensing techniques reported herein are employed to extrapolate carbon estimates over the study area with the following major objective:

»To compare remotely sensed derived biomass/carbon values to field measured aboveground woody biomass/carbon values for the purpose of finding out the reliability of estimating carbon sequestration from remotely sensed data.

*Other minor objectives include:*

»To test for the statistical significance of carbon sequestration's species dependence for the purposes of ascertaining the use of general conversion factors in converting oven-dry weight biomass to carbon amounts.

»To produce vegetation and carbon maps for Serowe-Botswana. These maps may be used in the informed decision making processes by the local authorities.

#### 1.4.2. Research Questions

- ▶ How accurate and reliable can remotely sensed carbon estimations be compared to actual field measured carbon values?
- ▶ To what extent do different species contribute to carbon sequestration?
- ▶ How much carbon is sequestered in Serowe's aboveground woody biomass?

#### 1.5. Hypotheses

##### 1.5.1. Field and Remotely Sensed Measurements

**H<sub>0</sub>** there is no difference between the mean total carbon (biomass) values obtained from remotely sensed data ( $C\mu_0$ ) and the mean total carbon (biomass) obtained from in-situ measurements ( $C\mu_1$ ), i.e.,  $(C\mu_0) = (C\mu_1)$ .

**H<sub>1</sub>** there is a difference between the two means (i.e., the mean total carbon (biomass) from remote measurements ( $C\mu_0$ ) and the mean total carbon (carbon) measurements from field in-situ ( $C\mu_1$ ) measurements), i.e.,  $(C\mu_0) \neq (C\mu_1)$ .

##### 1.5.2. Is Carbon Content Species Dependent?

**H<sub>0</sub>** the means of the carbon content measurements in all the ten species populations are equal (i.e., the carbon means are the same in all the ten species).

**H<sub>1</sub>** the carbon content means of the ten species populations are not equal (i.e., not all of the means are equal or the same).

## 2. THEORY AND PRACTICE OF THE ENERGY BALANCE EQUATION

### 2.1. The Energy Balance Equation

The exchanges of radiative, heat and moisture fluxes affect the biosphere development and physical conditions on earth (Bastiaanssen et al., 1998). These fluxes can be summarised in a form of the energy balance (*EBE*) equation below:

$$R_n = \lambda E + H + G_o \quad (W/m^2) \quad (2.1a)$$

$$R_n = K\downarrow - K\uparrow + L\downarrow - L\uparrow \quad (W/m^2) \quad (2.1b)$$

where  $R_n$  is the net incoming radiation;  $\lambda$ , the latent heat of evaporation;  $E$ , the rate of evaporation;  $H$ , the sensible heat flux into the atmosphere and  $G_o$ , the heat flux conducted into Earth,  $K$  the incoming short-wave radiation ( $0.3 - 3 \mu m$ ) and  $L$  the long-wave radiation ( $3 - 100 \mu m$ ). (Brutsaert, 1982); (Reginato et al., 1985) and (Bastiaanssen et al., 1998). The arrows indicate the flux direction. (Bastiaanssen et al., 1998) suggests that this equation neglects the energy required for photosynthesis and the heat storage in vegetation. How then does the *EBE* link with biomass and carbon estimation in this study?

#### 2.1.1. Energy and Biomass

Photosynthetically Active Radiation-*PAR* ( $0.4 - 0.7 \mu m$ ) is part of the incoming short-wave radiation ( $K\downarrow$ )-( $0.3 - 3.0 \mu m$ ) from the sun and is potentially useful for photosynthesis (Lillesand and Kiefer, 2000); (Bastiaanssen and Ali, 2001) and (NTSG, 2002). (Frouin and Pinker, 1995) and (Bastiaanssen and Ali, 2001) report that *PAR*, a fraction ( $PAR/K\downarrow$ ) of  $K\downarrow$ , varies with visibility, optical depth, ozone amount and cloud cover among others. However, they further suggest that a value of approximately 45 to 50% is generally accepted to represent a 24-hour average condition:

$$PAR = 0.48 * K\downarrow_{24} \quad (W/m^2) \quad (Bastiaanssen and Ali, 2001) \quad (2.2)$$

Because not all the available *PAR* is absorbed by the canopy and used for  $CO_2$  assimilation, Hartfield et al., (1984) and Asrar et al., (1992) in (Bastiaanssen and Ali, 2001) found that absorbed photosynthetically active radiation (*APAR*) could be computed as a rest term of the leaf balance radiation. This was done with respect to canopy reflectance, transmittance and the portion of the transmitted radiation that is reflected by the soil. *APAR* was thus directly approximated from *PAR* as:

$$APAR = f * PAR \quad (W/m^2) \quad (Bastiaanssen and Ali, 2001) \quad (2.3)$$

In (Daughtry et al., 1992) and (Bastiaanssen and Ali, 2001), it is stated that the  $APAR/PAR$  fraction ( $f$ ) changes non-linearly with the leaf area index. They further report that  $f$  can mathematically be derived from spectral measurements in the red and near-infrared spectral range as a remote sensing surrogate for leaf area index:

$$f = -0.161 + 1.257 * NDVI \quad (2.4)$$

where *NDVI* is defined as the difference between near-infrared and red reflectances divided by their sum.  $f$  (fractional photosynthetically active radiation-*FPAR*) is a measure of the proportion of the available radiation in the specific photosynthetically active wavelengths of

the spectrum that a canopy absorbs. (Bastiaanssen and Ali, 2001) give the accumulation of biomass according to the Monteith model with respect to accumulated *APAR* as:

$$\text{Tot. Acc. Biomass} = \varepsilon \Sigma(\text{APAR}(t) * t) \quad (\text{Kg m}^{-2}) \quad (2.5)$$

where *Tot. Acc. Biomass* is the accumulated aboveground dry biomass in a period  $t$ ;  $\varepsilon$  ( $\text{g MJ}^{-1}$ ) is the light use efficiency, growth efficiency, conversion efficiency, biological efficiency, or radiation use efficiency and  $t$  describes the period over which accumulation takes place. Equation (2.5) forms the base of the Carnegie-Ames-Stanford Approach (*CASA*) and this study's assumption that carbon can thence be measured from remotely sensed data.

### 2.1.2. The CASA Overview

The *CASA* is a simple terrestrial ecosystem model that combines satellite and surface observations in estimating annual net primary production and decomposition. It was first introduced by Potter et al., in 1993 and later expanded by (Field et al., 1995) to be able to convert the product of *APAR* and  $\varepsilon$  to net primary production (*NPP*) for a given area ( $x$ ) in time ( $t$ ). The modification was the incorporation of a structure that allows  $\varepsilon$  to vary seasonally and within biomes without recourse to ecosystem-specific  $\varepsilon$  values (Field et al., 1995) This structure is as depicted in the model below:

$$\varepsilon(x,t) = \varepsilon^\circ(x,t) * T_1(x,t) * T_2(x,t) * W \quad (\text{g MJ}^{-1}) \quad (2.6)$$

where  $\varepsilon$  is a corrected calculated variable in time and space;  $\varepsilon^\circ$ , the globally uniform maximum value;  $T_1$ , and  $T_2$  are temperatures depicting temperature suitability and  $W$ , the availability of water. These scalars are field calibrated where ( $W$ ) is a ratio of estimated evapotranspiration (*EET*) to potential evapotranspiration (*PET*) with a minimum value of 0.5. According to (Field et al., 1995) *CASA* assumes that each grid cell (pixel) is well drained thus not limiting productivity by anaerobic conditions in supersaturated soils. They also found out that *CASA*'s ability to track variation in crop yield was strongly dependent on *NDVI* data.

### 2.1.3. The SEBAL Overview

*SEBAL* is a process-based ecosystem algorithm that simulates important evapotranspiration and energy fluxes. (Bastiaanssen et al., 1998), give a detailed account on the formulation of this algorithm advancing ten sound reasons why it is considered better than other energy balancing algorithms. The account below gives a summary of *SEBAL*, which basically describes the latent heat flux ( $\lambda E$ ) as the rest term of the instantaneous surface energy balance (Bastiaanssen et al., 1998):

$$\lambda E(x,y) = f \{ r_o(x,y), K^\downarrow(x,y), \varepsilon'_2, \varepsilon_o(x,y), x T_o(x,y), G_o(x,y), Z_{om}(x,y), kB^{-1}, x u^*(x,y), L(x,y), \delta T_a(x,y) \} \quad (\text{W/m}^2) \quad (\text{Bastiaanssen et al., 1998}) \quad (2.7)$$

where  $r_o$  is the albedo;  $K^\downarrow$  ( $\text{Wm}^{-2}$ ) is the incoming solar radiation;  $\varepsilon'_2$  the apparent thermal infrared emissivity of the atmosphere;  $\varepsilon_o$  is the surface thermal infrared emissivity;  $T_o$  (K) the radiometric surface temperature;  $G_o$  ( $\text{Wm}^{-2}$ ) the soil heat flux;  $Z_{om}$  (m) the surface roughness length for momentum transport;  $kB^{-1}$  the relationship between  $Z_{om}$  and the surface roughness length for heat transport;  $u^*$  ( $\text{ms}^{-1}$ ) the friction velocity;  $L$  (m) the Monin-Obukhov length and  $\delta T_a$  (K) the near surface vertical air temperature difference. The  $(x,y)$  notation denotes that a particular parameter is variable in the horizontal space domain with a resolution of one pixel.

The above expression was adopted from (Bastiaanssen et al., 1998) and detailed accounts of each parameter are discussed therein.

#### 2.1.4. Energy Balance Equation-Relationships Between Carbon and Water

The partitioning of energy between the terms in equations (2.1a & b) is largely controlled by the availability of water in a system (Goward et al., 1985). It has further been elaborated by (Brutsaert, 1982), (Reginato et al., 1985); (Goward et al., 1985) and (Bastiaanssen et al., 1998) that aerodynamic diffusion and canopy resistances to water vapour transpiration and/or transport are important parameters in the energy exchange process over vegetated surfaces. The aerodynamic resistance is a complex function of wind velocity, stability of the atmosphere and plant height. See equations 2.19a and b.

*SEBAL* calculates  $\lambda E$  as a rest term of the instantaneous surface energy balance yielding an evaporative fraction ( $A$ ). This fraction is what is fed into the *CASA* model to yield total accumulated aboveground dry biomass ( $Kg/m^2$ ) in a period of time. According to (White, 2001) the relationship between photosynthesis and transpiration is based on phenomenological studies correlating changes in the assimilation of  $CO_2$  with changes in vapour pressure deficit ( $VPD$ )-the variable that is well represented in *SEBAL*. Most modern models of photosynthesis in fact pre-calculate the stomatal conductance based on the rate of  $CO_2$  assimilation modified by the sensitivity of the species to  $VPD$  (White, 2001).

(White, 2001) retorted that the evidence for coupling between  $CO_2$  and  $H_2O$  loss is based on looking at the changes in stomatal conductance with increases in internal  $CO_2$  concentration. Thence, this marks the core relationship between water,  $CO_2$  and biomass. This parabolically described functional relationship (Xiao et al., 2001) between atmospheric  $CO_2$  concentration and water ( $H_2O$ ) availability  $\{f(CO_2, H_2O)\}$  is computed as follows:

$$f(CO_2, H_2O) = \frac{C_i}{(k_c + C_i)} \quad (Xiao et al., 2001) \quad (2.8)$$

where  $C_i$  is the concentration of  $CO_2$  within the leaves of the canopy and  $k_c$ , the half saturation constant for  $CO_2$  uptake by plants and  $f(CO_2, H_2O)$ , a functional term in the gross primary production ( $GPP$ ) equation ( $C_{max} f(PAR)$ ,  $f(Leaf)$ ,  $f(T)$ ,  $f(CO_2, H_2O)$ ,  $f(NA)$  – refer to Xiao et al. 2001 for details). As internal  $CO_2$  increases, stomatal conductance decreases. How? Unsure but White (Pers comm.) suggested that it may have something to do with the formation of bicarbonate ions in the mesophyll cytoplasm which change the water potential within these cells. (Raich et al., 1991 in (Xiao et al., 2001), further went on to expound that the relationship between  $CO_2$  concentration inside stomatal cavities ( $C_i$ ) and in the atmosphere ( $C_a$ ) is directly proportional to relative moisture availability as depicted below another sound relationship between water and  $CO_2$ :

$$C_i = G_v C_a \quad (2.9a)$$

$$G_v = 0.1 + (0.9 * EET/PET) \quad (2.9b)$$

where  $G_v$  is a unit-less multiplier that accounts for changes in leaf conductivity to  $CO_2$  resulting from changes in moisture availability. Thus moisture availability governs the consumption of  $CO_2$  and its transfer through changes in wind speeds over canopies. Wind speeds (air in motion) are brought about by changes in air temperature, which are brought about by the influence of energy. To continue, in the above equation (2.9b),  $PET$  is potential

evapotranspiration and  $EET$  is the estimated evapotranspiration-just as in  $CASA$ . The flux  $PET$  is calculated as a function of mean air temperature and solar radiation (Field et al., 1995) and Jensen and Haise, 1963 in (Xiao et al., 2001).  $PET$  only depends on climatological factors. The flux  $EET$  is equal to  $PET$  in wet months but is modelled as a function of rainfall and a change of soil moisture in dry months (Goward et al., 1985; Field et al., 1995 and Vorosmarty, et al., 1989 in (Xiao et al., 2001). It is the real amount of water that is consumed by plants.

The above interactions emphasise the validity of measuring 'A' in estimating biomass and carbon from remotely sensed data in combination with  $CASA$ . (Moldenhauer and Lüdeke, 2000) report that the response of net primary production of terrestrial vegetation to climate change is central to global carbon cycling and climate impact research. This appears to be in conformity with what (Brutsaert, 1982) says, "Changes in the surface energy budget are related not only to climate changes but also to changes in water budget."

### 2.1.5. The Evaporative Fraction

The calibration of  $CASA$  involves the consideration of water and temperature as scalars calculated for all pixels for an entire model year. In  $SEBAL$  the land surface parameterisation is done for each pixel instantaneously. Nonetheless, this can be integrated into any time scale desirable although one day is often used. In  $CASA$ -modified, Field et al., (1995) applied a minimum value of  $W = 0.5$  and assumed that every grid was well drained. In this study, the evaporative fraction from  $SEBAL$  is used "to allow 'W' reduce to nil if the root zone is oven dry" (Bastiaanssen and Ali, 2001). The evaporative fraction ( $A$ ) in  $SEBAL$  is given as a fraction of the net radiation (surface energy balance) per day as illustrated below:

$$W = A = \frac{\lambda E}{R_n - G_o} \quad (\text{Bastiaanssen and Ali, 2001}) \quad (2.10)$$

Energy, flows through the ecosystems as heat continually driving abiotic and biotic processes. As already stated the partitioning of this energy between processes is largely controlled by the availability of water in the system. As is recorded, when moisture is not restrictive, ' $\lambda E$ ' reaches a maximum while sensible heat ( $H$ ) tends to zero. The flow of ' $H$ ' in a flux as applicable in the  $EBE$  theory is represented as:

$$H = \rho_a * C_p * \frac{T_o - T_a}{r_{ah}} \quad (2.11a)$$

Where;  $\rho_a$  is the moist air density ( $kg\ m^{-3}$ );  $C_p$  the air specific heat at constant pressure ( $J\ kg^{-1}\ K^{-1}$ );  $r_{ah}$  is the aerodynamic resistance of heat transport between the surface and the reference level ( $s\ m^{-1}$ ) see equation (2.19a);  $T_o$  is the surface temperature while  $T_a$  is the air temperature. As Meijerink in lecture notes says, the evaluation of ' $r_{ah}$ ' is the most complicated part in the whole of  $EBE$  procedure for evapotranspiration estimates.

The above equation is solved iteratively as ' $r_{ah}$ ' varies with wind speed and the intensity and direction of ' $H$ ' among other variables i.e., ' $r_{ah}$ ' =  $f(H)$ , where ' $H$ ' becomes as shown below:

$$H = \rho_a * C_p * \frac{T_o - T_a}{f(H)} \quad (2.11b)$$

The evaporative fraction ( $A$ ) is defined as the energy used for the evaporation process divided by the total amount of energy available for the evaporation process:

$$A_{inst} = \frac{\lambda E}{\lambda E + H} = \frac{\lambda E}{R_n - G_o} \quad (2.12a)$$

See equation (2.1a) for the description of the terms used above.

$$A_{day} = \frac{\lambda E_{day}}{Rn_{day} - G_{day}} \quad (2.12b)$$

During the period of 24 hrs,  $G_{day}$  tends to zero thus it may be cancelled out giving the final evaporative fraction equation as:

$$E_{day} \text{ (mm/day)} = \frac{Rn_{day} * A_{inst}}{28.8} \quad (2.13)$$

where;

$$A_{inst} = A_{day} \quad (2.14)$$

An evaporative fraction has a range of zero to one and an evaporative fraction of 0.2 means 20% of the energy was used to convert water into vapour.

### 2.1.6. Other Key Variables for Energy Balance Equations

Key variables for water-energy-carbon algorithms include: albedo ( $r_o$ ), incoming solar ( $K\downarrow$ ) and longwave ( $L$ ) radiations. In remote sensing these variables can be expressed as a thermodynamic equilibrium in the form of an electromagnetic spectral balance of all incoming and outgoing fluxes reaching and leaving the earth's surface as represented in equation (2.1b). In line with that equation, the other parameters are computed by the formulas shown in the table below.

Variable	Equation	Equation serial number
Outgoing longwave radiation	$L \uparrow = \sigma \epsilon_o T_o^4$	2.16
Incoming longwave radiation	$L \downarrow = \sigma \epsilon'_a T_a^4$	2.17
Emissivity of the atmosphere	$\epsilon'_a = 1.24 * (e_a / T_a)^{1/7}$	2.18

**Table 2.1: Other key EBE variables.**

From the table,  $\sigma$ , is the Stefan-Boltzman constant ( $5.67e-8 \text{ Wm}^{-2}\text{K}^{-4}$ );  $\epsilon_o$  is the broadband emissivity measured in situ or derived from surface properties;  $T_o$  derived from radiant temperature  $T_{rad}$ ;  $T_a$ , the air temperature;  $\epsilon'_a$  is the apparent emissivity of the atmosphere; and  $e_a$ , the vapour pressure (mbars).

Other key variables include soil temperature ( $^{\circ}\text{C}$ ), wind speeds ( $\text{m/s}$ ) and relative humidity (%) measurements. The determination of evapotranspiration and heat transfer phenomena (sensible heat flux) requires the description of the turbulent wind profile near the Earth's surface. This turbulent wind profile is dependent upon the aerodynamic conductance, into

which the surface roughness parameters enter logarithmically. A simple representation of a stability corrected aerodynamic resistance ( $r_{ah}$ ) is found in (Reginato et al., 1985) and represented below:

$$r_{ah}(x,y) = r_a \{1 - n(z-d) * (T_s - T_o) / (T_o u^2)\} \quad (2.19a)$$

where  $r_a$  is:

$$r_a(x,y) = \{\ln[(z-d)/z_o]\}^2 / (k^2 u) \quad (2.19b)$$

where  $n$  is a constant usually assumed to be five;  $z$ , the reference height ( $m$ );  $d$ , the displacement height ( $m$ );  $T_s$ , the surface temperature ( $^{\circ}C$ );  $T_o$ , the air temperature ( $^{\circ}C$ );  $z_o$ , the roughness length ( $m$ );  $T_o$ , the average of the air and surface temperatures ( $K$ );  $u$ , the wind speed ( $m/s$ ) and  $k$  a constant = 0.41. According to (Reginato et al., 1985), equation (2.19a) gives a reasonable estimate of the aerodynamic resistance for low to moderately unstable conditions.

## 2.2. Biomass Calculation from SEBAL and CASA algorithms.

A theoretical summary of the steps involved in the calculation of biomass from remote sensing data is as outlined below (Samarasingha, 2000):

$$\begin{aligned} \text{NDVI} &= f(\text{Band 4, Band 3}) && \text{(Tucker, 1979)} \\ \text{Biomass} &= f(\text{APAR}) && \text{(Kumar and Monteith, 1981 in (Samarasingha, 2000))} \\ \text{FPAR} &= f(\text{NDVI}) && \text{(Daughtry et al., 1992)} \\ \text{PAR} &= f(K \downarrow) && \text{(Christensen and Goudriaan, 1993)} \\ \text{Biomass} &= \text{APAR} * \varepsilon && \text{(Field et al., 1995)} \end{aligned}$$

where  $\varepsilon$  = light use efficiency

$$\varepsilon = \varepsilon^{\circ} * T_1 * T_2 * W, \quad \text{(Potter et al., 1993; (Field et al., 1995))}$$

where  $\varepsilon^{\circ}$  = globally uniform maximum (2.5g/MJ) and

$T_1$  and  $T_2$  relate to plant growth regulation (acclimation) by temperature where

$$T_2 = 1.185 * \{1 + \exp(0.2T_{opt} - 10 - T_{mon})\}^{-1} * \{1 + \exp(-0.3T_{opt} - 10 + T_{mon})\}^{-1} \quad \text{(Field et al., 1995)}$$

where

$T_{opt}$  = mean temperature during the month of maximum *NDVI* (constant for a certain vegetation type during the season), and

$T_{mon}$  = mean monthly air temperature.

$$T_1 = 0.8 + 0.02 * T_{opt} - 0.0005 * (T_{opt})^2 \quad \text{(Field et al., 1995)}$$

$$W = 0.5 + (EET/PET) \quad \text{(Field et al., 1995)}$$

$W = A$ , the evaporative fraction from *SEBAL*. (Bastiaanssen and Ali, 2001)

Therefore, **Biomass** =  $APAR * \varepsilon * T_1 * T_2 * A$

### 2.3. The difference between Production and Productivity

Primary Productivity is measured as the rate of formation of new materials per unit of Earth's surface and per unit of time (Umich, 2001). It may either be reported as *calories cm<sup>-2</sup> yr<sup>-1</sup>* in energy terms or as *gm<sup>-2</sup> yr<sup>-1</sup>* (dry organic matter). The unit (*1/time*) distinguishes productivity from standing plant biomass, which is simply the amount of matter found in a given area at any point in time (*g m<sup>-2</sup>*). Thus, when production is calculated, accrual over time is accounted for. Standing plant biomass on the other hand is a measure of matter at a single point in time. This difference between productivity and standing plant (production) is a very crucial one not only in this study but the subject of carbon sequestration as a whole.

In environmental systems analyses, the point in time when one begins measurements is usually considered as point zero, the (initial state) (Dingman, 1994). Increase or decrease in the state of the substance at hand will only be determined at the next measurement at the same place. This is where the concept of permanent plots in carbon sequestration projects comes in i.e., knowing how much carbon has been stored at a given place in a given time.

### 3. DESCRIPTION OF THE STUDY AREA

#### 3.1. Location

Serowe, one of the largest villages in Southern Africa, is administratively located in the Central District of Botswana. It is some 300 km NE of Gaborone with local latitude of  $22^{\circ} 23'$  (UTM coordinates being: 410000, 7650000 and 490000, 7510000). See figure 5.2. The topography of this study area ranges from a relatively higher flat portion of land in the west (sandveld), an escarpment and the lower area in the east (hardveld) covered by dark sandy clay-loamy soils, river channels and scattered hills. The escarpment cuts the study area almost into two halves. It stretches from north to south and imposes an altitude fall of approximately 100 m between the two velds at the highest point.



Apart from the main Serowe village, the study area contains a few isolated and sparsely populated human settlements. Just like in the whole of Botswana, cattle rearing is one of the main activities from the earliest of times. It is sustained by an extensive savannah vegetation and groundwater from boreholes locally known as cattle-posts in their animal husbandry practice. Coupled with good veterinary science practice and stock breeding programmes, this area too has a sustained animal industry.

**Figure 3-1: The relative position of the study area.**

#### 3.2. Climate

The climate of the study area is characterized by a mean annual rainfall of 447 mm (SGS, 1998 and Vossen, 1989 in (Obakeng, 2000) and mean temperature of about  $21.3^{\circ}\text{C}$  with mean relative humidity ranging between 40% and 65%. In climatic classification terms, the area falls in the category of semi-aridness with an average altitude of 1150 m above sea level.

Below are two graphs of daily temperature measurements at Mahalapye, the nearest official meteorological station and daily wind speed measurements at Serowe respectively.

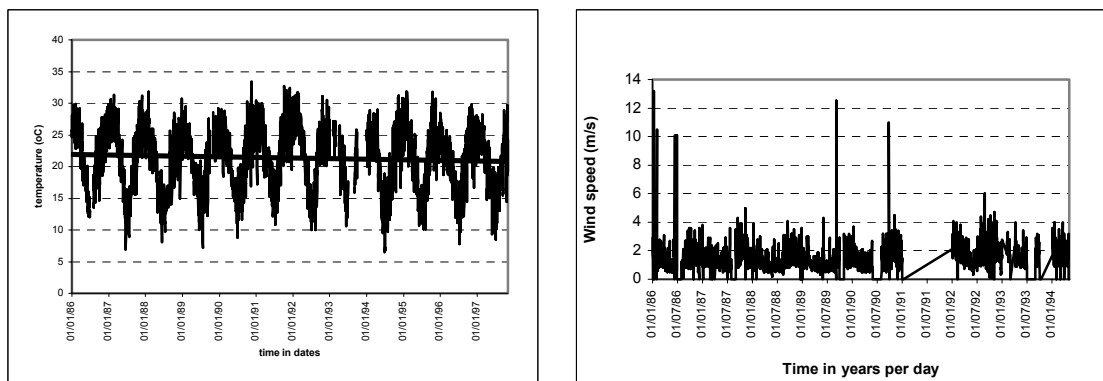


**Figure 3-2: Daily measurements of temperature and wind speed respectively from 01/01/86 to 01/01/94. Note data gaps in the wind speed graph.**

### 3.3. Vegetation

Serowe's vegetation is part of the Zambebian Phyto-Region that lies between latitudes  $3^{\circ}$ - $26^{\circ}$  S and extends from the Atlantic to the Indian oceans. The Serowe biomass resource depicts a typical semi-arid savannah environment with average tree height ranging between 3 m to 5 m. Although (FAO, 2001) defines a tree as any form of woody vegetation able to reach a minimum height of 5 m at maturity in situ, a tree is defined as any woody plant above 3 m of stature in this study. The vegetation exhibits spread sparse canopies that are sometimes dense and multi-stemmed stem habits.

On the plateau covered by the Kalahari sands, the vegetation is mainly shrubs showing community homogeneity but least density. The escarpment and the lower veld (hardveld) show relatively higher plant densities. Although the dominant type of vegetation in Serowe is open savannah, this may be subdivided into three cover types viz., open shrub grassland (Plateau-Sandveld), scrubby bushy woodland/woody scrubland (lower woody bushveld-Hardveld), and the hilly shrub-woodland (escarpment hinterland and faces), (Ecosurv, 1998) and (Timmermans and Meijerink, 1999) give a detailed description of vegetation in the study area.

Close to the escarpment, the vegetation becomes green, dense, tall and big in terms of stem diameter. The existence of such dense woodland on the escarpment is poorly understood. (Timmermans and Meijerink, 1999) found no association between groundwater depth and vegetation density on the plateau. They thus, suggested, a possible influence from seasonal perched water tables in the distribution of the vegetation. However, from field observations, it was noted that the escarpment soils have high moisture retention capabilities and so are the rocks.

Spiny acacias with mosaics of other tree/shrub species dominate the drier parts of the study area especially the hardveld and sandveld whereas their existence among the escarpment vegetation is compromised. A total number of 28 tree and shrub species were recorded (See appendix AI). In this semi-arid environment, trees were often short and fat or tall and thin. At the time of the study, the area exhibited evidence that no bush fire had affected it in a very long time but that it had been grazed upon.



**Figure 3-3: Escarpment (left) and hardveld (right) vegetation. September 18, 2001.**

Closer to the escarpment, the terrain becomes more undulating and local depressions occur as can be seen from pictures 3.3 (left). In the hardveld (right picture) the vegetation is typically multi-stemmed and leafless as typically depicted in the right photograph. Soils and soil moisture conditions vary greatly (Timmermans and Meijerink, 1999), causing a mixture of habitats with a large number of different plant communities.

### **3.4. Coal Mining and Power Generation**

In relation to the essence of the subject matter of this research study, there is located to the east just outside the study area boundary, Botswana's largest and long future source of a fossil fuel (coal). Morupule Colliery Limited, an underground mine (70 m deep), produces medium grade bituminous coal, aged at 200 million years that is supplied to the nearby Morupule Power Station. The power station is of a capacity of 133 MW of electricity generation supplying the whole country.

## 4. METHODS AND MATERIALS

### 4.1. Pre-fieldwork

Prior to fieldwork, an intensive and extensive literature review was conducted. The pertinent findings were as outlined in chapter two. Field measurable variables for the algorithms and field biomass estimations were enumerated. Suitable measuring instruments were thence prescribed and acquired. The August 11 2000 *Landsat-7 ETM+* satellite images were used in the pre-fieldwork studies including the calculation of *NDVI*. Earlier studies show that the study area's vegetation could be divided into three vegetation cover classes based on the locality (Ecosurv, 1998). Therefore, a stratified random sampling (*StRS*) design was chosen in line with further literature review (MacDicken, 1997) for more precise estimates at a fixed cost. Three other options that were reviewed included: complete enumeration, simple random sampling and systematic sampling. Hence, the study area was divided into three strata-sandveld, hardveld and escarpment.

The randomisation (sample distribution) of the sampling plots was done using the random function of a computer to select centre coordinates based on a false colour composite bands-453 in reference to the *NDVI* map. In order to compare the efficacy of remote sensing in estimating carbon sequestered in the study area, field aboveground measurements of biomass must be done. This requires cutting down the vegetation, but fortunately in this study, allometric equations were found to exist for the study area during the literature review.

#### 4.1.1. Sampling Design

A sampling design of sampling units of size  $60\text{ m} \times 60\text{ m}$  ( $3\,600\text{ m}^2$ ) was framed. The sampling unit size was decided upon in recognition of the sparsity of the vegetation in the study area and the need of a uniform spatial and radiometric plot size for sound comparison with remote sensing techniques. All the spectral bands of the *Landsat-7 ETM+* images were resampled to the pixel size of the thermal band (*six*) and given the same georeference. Thence, the sampling units on which observations were made were based on a fixed-area-plot size.

Each pixel ( $60\text{ m} \times 60\text{ m}$ ) was treated as one unit having the same chance of being selected. The identification of each pixel was according to its row and column position. These were then coded e.g. *Pixel (1,1) as 001001*. These six digits random numbers were then randomly regenerated using a computer and their coordinates recorded as the centre of a plot. These coordinates were thence used to delineate the selected plot centres in the field. The false colour composite image (*453*) map was superimposed on the randomly stratified sampling plot cites and printed for use in the field.

(Lemenih, 1995) reports that 50 sample plots are usually sufficient to establish a good tree biomass/tree variable relationship. However, in this study 60 plots were initially designed but 23 more were defined while in the field. The initial 60 plots were equally distributed over the three strata due to the large size of the study area (*244 048 hectares*). In line with this number of plots, a margin of error of no larger than 0.51 would have to be accepted at 95% confidence level and a standard deviation of two. With the extra 23 plots, the margin of error must fall but the above margin of error was maintained for this study. In order to cater for the biomass estimation of shrubs, sub-sampling plots of size  $5\text{ m} \times 5\text{ m}$  were selected within the  $60\text{ m} \times 60\text{ m}$  sample plots based on expert judgement.

The sub-plots of  $5\text{ m} \times 5\text{ m}$  delineated to cater for the estimation of shrub fresh weight biomass were equal in number with the bigger plots ( $60\text{ m} \times 60\text{ m}$ ). To verify the use of the commonly used conversion factor of 0.5 from biomass to carbon (MacDicken, 1997) in Serowe, 50 tree and shrub branch samples were selected from within the big plots for the 10 most common species. Branches of the trees and shrubs were selected recognising the fact that different parts of these organisms would have different quantities of carbon at different stages in their life histories. Hence, branches were thought to represent an average of the carbon content in both trees and shrubs and thus allow for the carbon content comparison.

#### 4.1.2. Allometric Biomass Equations

These are regression equations that provide a relationship between tree fresh weight biomass and a tree dimension(s). These equations for calculating stem biomass per tree vary widely with varied mathematical formulations. (Kilawe et al., 2001) gave the reasons for this variation. (Tietema, 1993)'s equations are based on a log-log transformation yielding power linear regression curves that gave the constants 'a' and 'b' as illustrated below:

$$B = a \cdot BA^b \quad (4.1)$$

where:  $B$ , is the fresh weight biomass ( $kg$ );  $BA$ , the basal area of a given tree stem ( $cm^2$ ) and 'a', 'b', being constants depending on the tree species. Thus, in accordance to Tietema's equations, the tree dimension used and recommended for Botswana, was a tree's basal area ( $BA$ ) computed from a tree's ankle height ( $5-10\text{ cm}$  above ground level) diameter measurement. See appendix AII for these regression equations.

#### 4.2. Fieldwork

In the field, a reconnaissance survey of the study area was done. A Garmin *12X-GPS*, in reference to the false colour composite satellite image map, was used to delineate the sampling plots using the centre coordinates. A  $50\text{ m}$  long tape was used to measure a distance of  $30\text{ m}$  from the centre in four compass directions with a northeastern orientation for all plots. Within the  $60\text{ m} \times 60\text{ m}$  plots, all woody plants of height three meters and more were measured for their ankle height diameter ( $AHD$ ) using a calliper ( $60\text{ cm}$  maximum arm-length) or a diameter tape ( $3\text{ m}$  maximum). Measuring on two perpendicular axes, the calliper arm pointed towards the centre of the plot at each first measurement in order to avoid systemic errors.

In estimating the shrub fresh weight biomass, all the woody vegetation in a sub-plot was cut and weighted using a spring balance. The measured weight was multiplied by 144 ( $3600\text{ m}^2/25\text{ m}^2$ ) in order to obtain the shrub fresh weight biomass representative of all the shrubs in the bigger sampling plot. In the same plots tree/shrub branches were purposively selected. These were cut, put in colourless transparent polythene bags, labelled and transported to South Africa for laboratory determination of oven-dry carbon content. This was done in order to answer research question number two. To minimise biasness, samples were collected from all the three strata as representative as possible.

Due to the use of the allometric equations and readily available assistance from the Geological Survey Department employees, time was saved and used in the sampling of the extra 23 plots

in addition of the designed 60. More of these plots were allocated to the Hardveld stratum because it exhibited more heterogeneity in the reconnaissance survey.

#### 4.2.1. Tree Cover, Species and Height

Tree crown cover was measured using a 30 m long tape on two perpendicular axes while tree height was estimated using the Haga hypsometer. Altitude, slope and pressure were also measured for a few sample plots. These were measured using an altimeter, and a clinometer. Trees that were found to branch below ground level were considered to be multi stemmed and the stems considered being individuals. The services of a local botanist were extensively utilized in identifying the tree species in local botanical names, which were later translated into scientific names according to (Moll and Moll, 1994) and (Palgrave, 1993). For the full list of tree species investigated, see appendix *AI*.

#### 4.2.2. Meteorological Measurements

Incoming solar radiation ( $K\downarrow$ ), temperature ( $T$ ), relative humidity ( $RH$ ), wind speed ( $u$ ) and soil temperature ( $T_{so}$ ) were measured using an Automated Data Acquisition System (*ADAS*). This automatic mobile weather station was shifted four times while in the field collecting data of the above-mentioned parameters at intervals of 30 minutes. Such an interval of data recordings may attenuate the effects of wind gustiness on the calculations of actual evapotranspiration as suggested by (Reginato et al., 1985).

The resultant data set in combination with satellite data is needed for the calculation of aerodynamic resistance to evaluate sensible heat and the evaporative fraction in the *SEBAL* algorithm. The table below outlines these variables in their standard units of measure and height at which the measurements were observed.

Climatic Parameters		
Variable	Instrument used	Measurement height (m)
Temperature (°C)	Shielded thermocouple	0.2
Temperature (°C)	Shielded thermocouple	2
Relative Humidity (%)	Shielded Hygrometer	0.2
Relative Humidity (%)	Shielded Hygrometer	2
Wind Speed (m/s)	Cup anemometer	0.2 and 2
Incoming Solar radiation (W/m <sup>2</sup> )	Pyranometer	2
Soil temperature (°C)	Soil thermometer	0.05
Soil temperature (°C)	Soil thermometer	0.15

**Table 4.1: *ADAS* measured parameters.**

Climatic data was also obtained from the Botswana Meteorological Department for the nearest weather station-Mahalapye. The data was used to study the climatic pattern and compare with the results from the *ADAS* loggers. Chapter three figure 3.2 shows the temperature and wind speed patterns of the study area.

### 4.3. Post fieldwork Activities

Activities after fieldwork included, the ordering of data, computations of some values to be used in the analyses such as the 0.5545 factor for the conversion of fresh weight woody biomass to oven-dry weight biomass. All variates were tested for normality prior to their use. Several statistical tests including the ANOVA, student-t-test and regression statistics were used throughout the study to observe the relationships and effects of the data on each other.

All statistical analyses were conducted using the Minitab-13 version 8.0 and Microsoft Excel-98 statistical packages. ILWIS-Academic-3.0 was used for all the satellite images calculations and map making.

#### 4.3.1. Tree Cover (%)

Tree cover was calculated as the sum of all the individual tree crown-areas divided by the area of the sampling plot multiplied by 100. On the assumption that trees in the semi-arid region rarely have multi-canopies, tree cover was tried as a surrogate of the LAI in the calculation of the displacement height ( $d$ ) required for SEBAL calculations. This was done in equation 4.2 below. In the equation, LAI requires one coefficient to adjust so as to fit a wide range of field results (Brutsaert, 1982) and is given as 20.6:

$$d = h * \left\{ 1 - \frac{1 - \exp(-\sqrt{cd * LAI})}{\sqrt{cd * LAI}} \right\} \quad (4.2)$$

where;  $h$  is the vegetation height ( $m$ ),  $cd$  the free parameter equal to 20.6 as default and LAI the leaf area index. Average tree height was computed for each stratum. To get the average height of the vegetation in the entire study area (see table 5.2 in the next chapter), the three averages were averaged.

### 4.4. Field Biomass Estimations of Aboveground Woody Vegetation

From the allometric equations described above, aboveground woody fresh weight biomass was calculated as a sum of all the individual tree biomasses in the sampling plots. However, the total woody biomass per sampling plot was a sum of the total individual tree biomasses and the shrub estimate of fresh weight biomass in the same plot. The biomass was converted from kilograms per plot to tons per hectare as shown in equation (4.3):

$$weight(kg)/3600m^2 = kg/m^2 = 10^{-3} \text{ tons}/10^4 \text{ ha} = \underline{10 \text{ tons/ha}} \quad (4.3)$$

yielding a conversion factor of 10 tonnes/ha. Another conversion factor of 0.5505 was used to convert fresh weight woody biomass to oven-dry biomass (see appendix BI) from which the carbon amounts were computed using a factor of 0.43 specific to Serowe.

Of the vital tree variables measured (height, crown diameter and AHD), AHD was used in the regression equations (appendix AII). An average of the two AHDs (measured on two perpendicular axes) was employed to compute the Basal Area (BA) in square-centimetres ( $cm^2$ ) to yield fresh weight biomass in kilograms per tree. The flow chart below displays the steps undertaken in the estimation of biomass and ultimately carbon in t/ha.

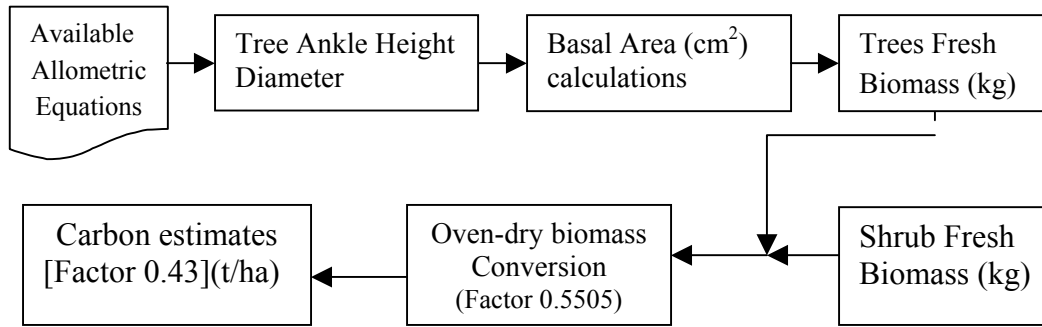


**Figure 4-1: Field biomass/carbon flowchart.**

#### 4.4.1. The Dumas-Method- Laboratory Analysis for Carbon Content

Five randomly distributed branch samples per tree/shrub species of the ten most common species in the study area were collected. These branch pieces were approximately seven centimetres in length with a mean diameter of 5.5 cm. The samples were sent to South Africa’s Forest and Forest Products Research Centre (*CSIR*) laboratories for oven-dry carbon content analysis. See appendix *AIII* for details and associated results.

The laboratory method used in the analysis of the amount of carbon in the samples was the *Dumas-Method* using the *Leco CNS 2000 Analyser*. This dry combustion method determined the total carbon content as oven-dry ratios. A sample was burnt at a temperature of  $1350^{\circ}\text{C}$  in a horizontal furnace converting all the elemental carbon, sulphur and nitrogen that may have been contained in the sample into  $\text{CO}_2$ ,  $\text{SO}_2$ , and  $\text{NO}_x$  respectively. In the ballast tank, these gases were homogenized and passed through infrared detection cells for the determination of the carbon and sulphur content. Details of this method can be found in (Matejovic, 1996).

#### 4.4.2. Biomass and Carbon Estimation from Remotely Sensed Data.

Below is a flow chart describing the steps taken in estimating biomass and carbon from satellite images:

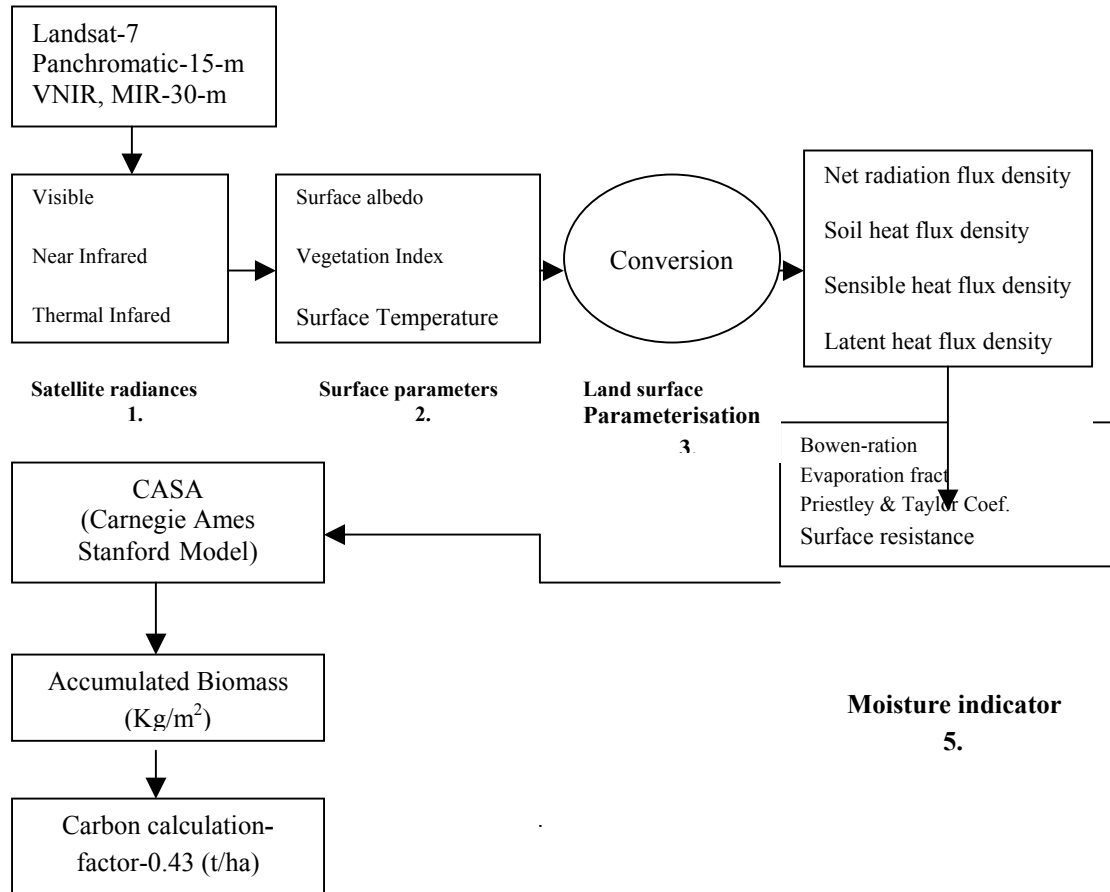


**Figure 4.2: Sequential steps in the determination of carbon from remotely sensed data. Components 1 to 5 have been adopted from (Bastiaanssen et al., 1998).**

The biomass estimation from remotely sensed data was calculated according to equation 4.4 below in reference to section 2.2 in chapter 2:

$$Biomass = APAR * \epsilon * T_1 * T_2 * A \quad (4.4)$$

#### 4.5. Field Biomass and Remotely-Sensed Biomass

In theory, two main methods are employed (see figure 4.2) herein running parallel to each other. These are field woody biomass estimation and a series of *remote sensing based algorithms* to estimate biomass and later on carbon. The figures below give an overview of the methods used from a raw data status to the final results, the correlative accuracy of remote sensing and field assessments, and vegetation and carbon maps. For another study area or under different circumstances (availability and stage of pre-processed data), the methods may have to be adjusted.

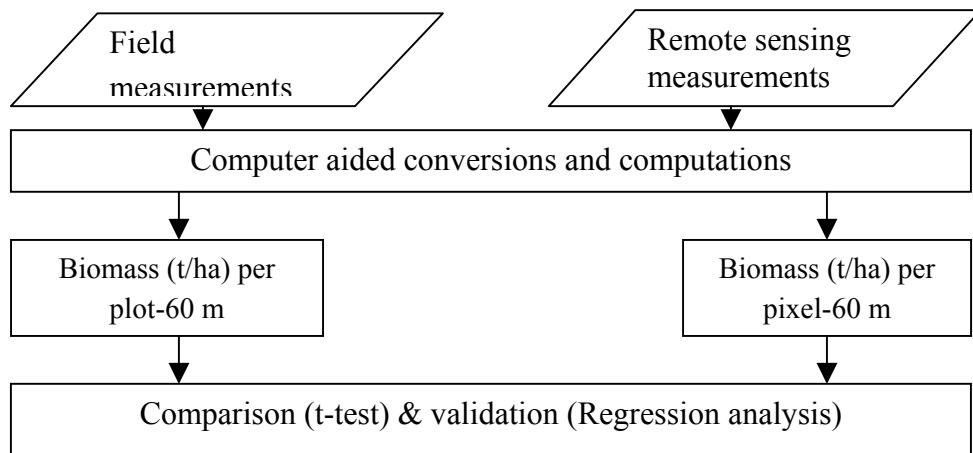


**Figure 4.3:** *Theoretical construction of the comparison and validation of the two approaches..*

#### 4.5.1. Assumptions

In performing the accuracy or comparison test, a number of assumptions were made and these include:

- that Tietema's allometric equations are accurate and applicable to the current study.
- that the sub-sampling plots ( $5\text{ m} \times 5\text{ m}$ ) were indeed representative of the shrub structure and cover in the bigger sampling plot.
- that Kaborč's derived fresh-dry weight biomass ratio applies to the Serowe situation.
- that the laboratory results on the oven-dry carbon content analysed using the single-factor-ANOVA analysis was normally distributed.

## 5. RESULTS

### 5.1. General

In order to describe, analyse and compare measured variables in the field, all the data sets were tested for normality. See appendix *BV* for details. In total, 83 plots were surveyed. Below are the results of the tree height analysis:

#### Descriptive Statistics: Tree Height (m)

Variable	N	Mean	Median	TrMean	StDev	SE Mean
Tree Hei	1386	4.7072	4.5000	4.5697	1.3021	0.0350
Variable	Minimum	Maximum	Q1	Q3		
Tree Hei	3.0000	14.0000	4.0000	5.0000		

**Table 5.1: Tree height statistics for the study area.**

Stratum	Min height (m)	Max height (m)	Average (m)
Sandveld Open Savannah	3.2	7.0	4.3
Hardveld Acacia Savannah	3.0	18	4.7
Escarpment Woodland	3.0	13.5	4.8
<b>Entire Sample Population</b>	<b>3</b>	<b>14</b>	<b>4.6</b>

**Table 5.2: Physical height of the vegetation per stratum.**

#### 5.1.1. Tree Cover (%)

Tree canopy cover was found to vary from 0% to 56% with an average of 11%. The table below gives a better picture about the frequency of tree canopy cover on sampling plots surveyed in relation to tree canopy cover class:

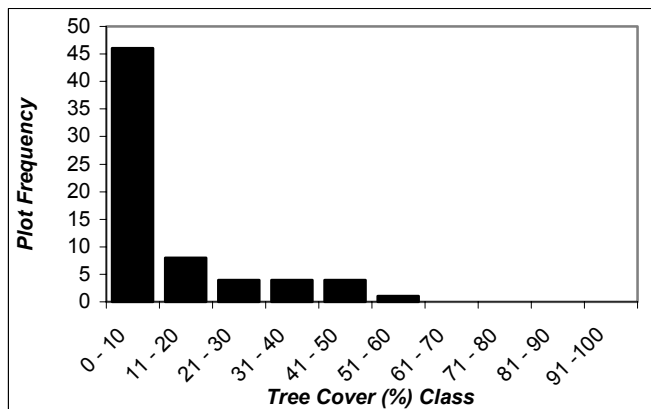


**Figure 5.1: Tree cover (%) frequency per cover class.**

#### 5.1.2. NDVI as an Indicator of Biomass

Spectral radiances of bands 4 and 3 of *Landsat-7 ETM+* of August 11 2000 gave the *NDVI* map as displayed in figure 5.2.

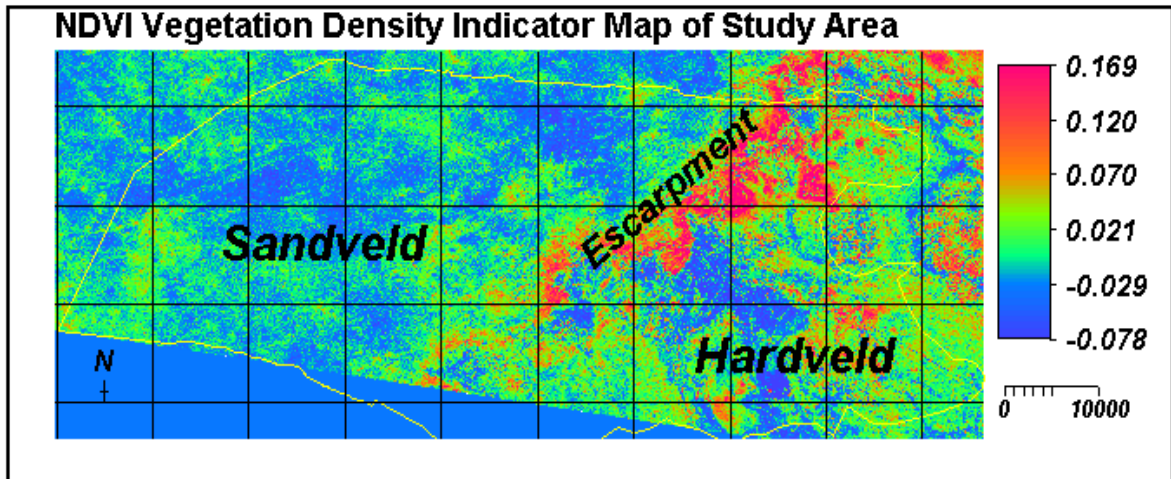


Figure 5.2: NDVI (bands 3 & 4) combinations from Landsat-7 ETM+ of August 11 2000.

### 5.1.3. Meteorological Results

The graphs below display the air temperature ( $^{\circ}\text{C}$ ), incoming solar radiation ( $K_{\downarrow}$ ) in  $\text{W}/\text{m}^2$ , relative humidity (%), and soils temperature ( $^{\circ}\text{C}$ ) from 10/08/2000 to 12/08/2000 respectively.

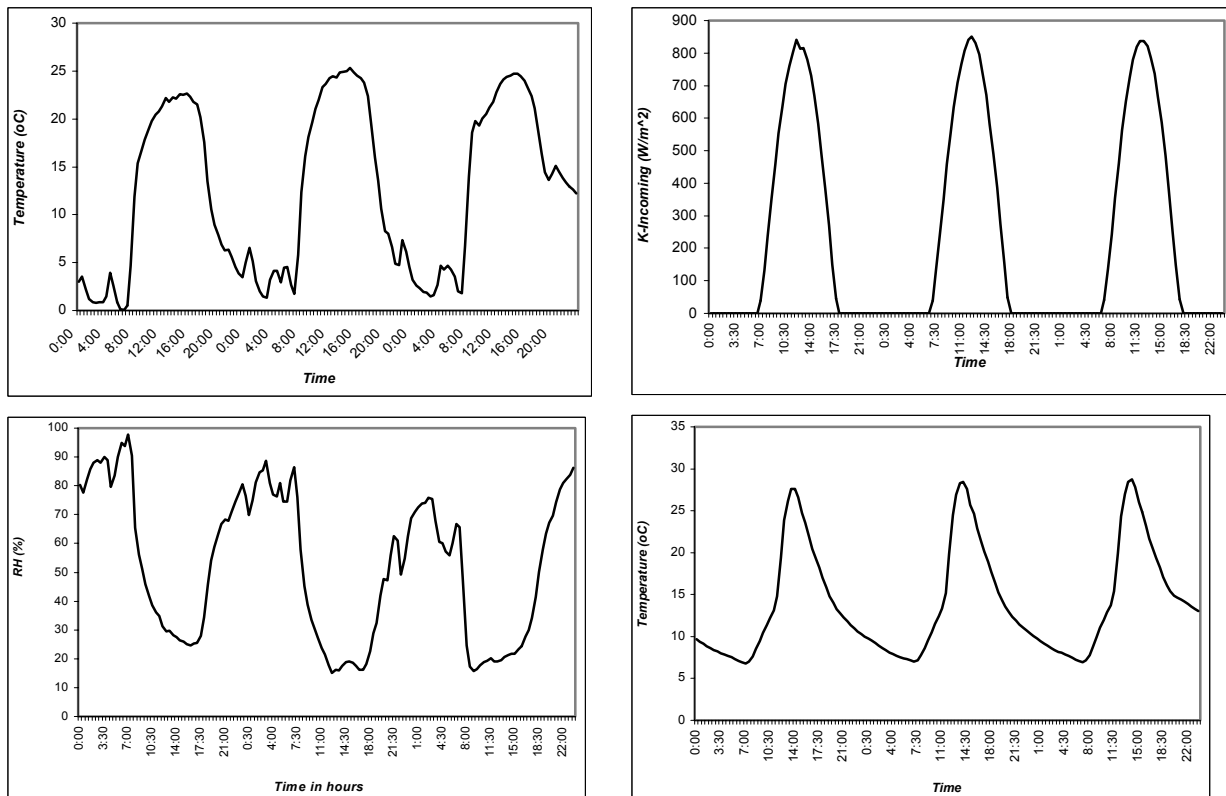
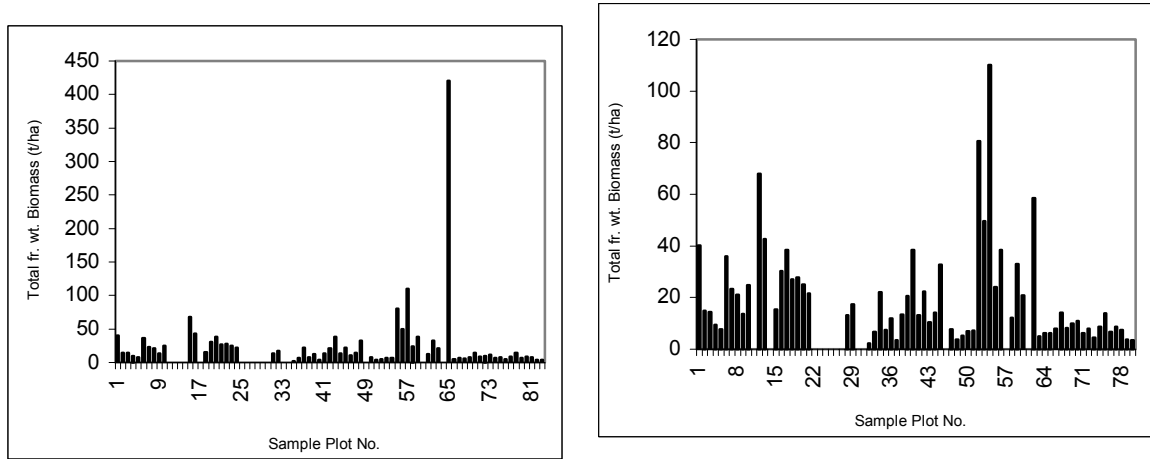


Figure: 5.3: (left to right, top)-air temperature and incoming solar radiation; (left to right, bottom)-relative humidity and soil temperature.

## 5.2. Field Biomass Estimation of Aboveground Woody Vegetation

The field estimated total fresh weight biomass for all the 83 plots was found to be as displayed below:



**Figure 5.4:** Total fresh weight biomass per sample plot with and without the outlier in plot 65 respectively.

Having corrected for the sampling unit outlier (riparian woodland tree- with a stem diameter of 3.6 m and a height of 14 m), in sample plot 65, and removal of three plots in the hardveld stratum to reduce the variance, the results become as shown below:

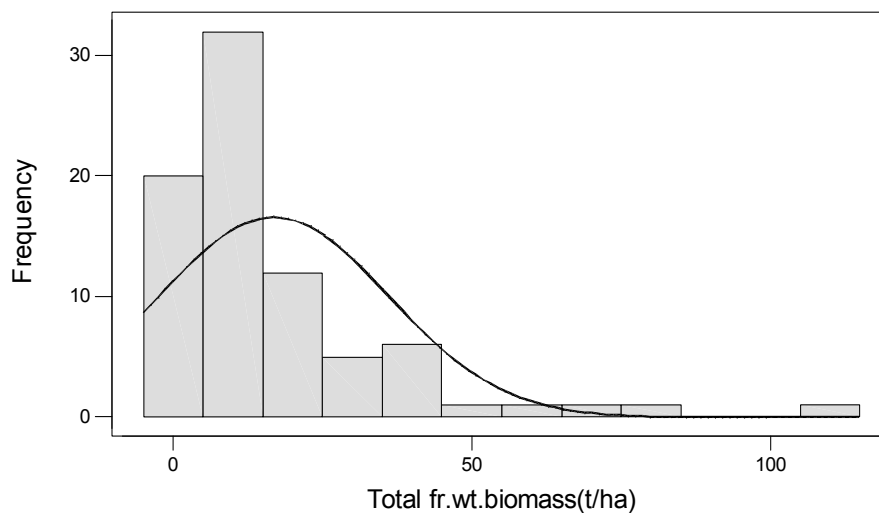


**Figure 5.5:** Frequency of total fresh weight biomass with Normal Curve.

The figure below displays the results of the total fresh weight above ground biomass per stratum with  $N = 80$ , sandveld  $n = 27$ ; hardveld  $n = 30$  and escarpment  $n = 23$ :

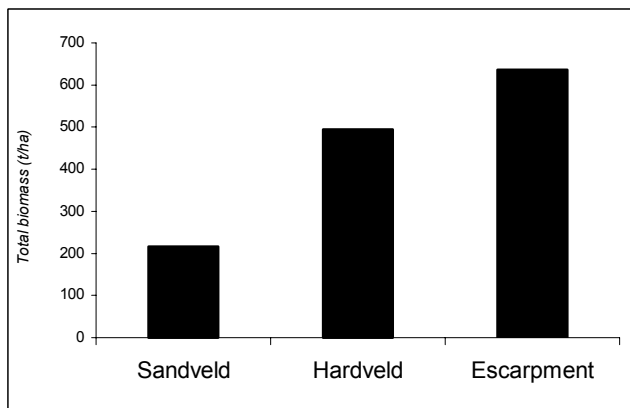


**Figure 5.6: Total fresh weight biomass per stratum.**

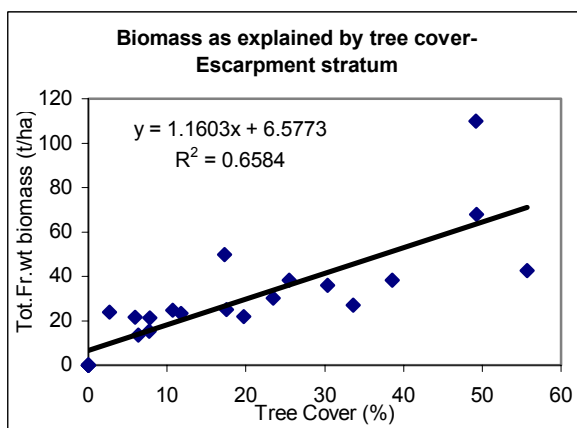
Results of the stratified random sampling analysis of the three strata for fresh weight aboveground woody biomass was found as shown in table 5.3 below:

Stratum	Sandveld	Hardveld	Escarpment	Population
<i>n</i>	27	30	23	80
<i>Variance</i>	10.652	358.022	623.513	
<i>Standard error</i>	0.628	3.455	5.207	1.294
<i>Sampling error % (p = 0.05)</i>	16.1	42.9	39.0	19.8
<i>Mean (tons. ha<sup>-1</sup>), (p = 0.05)</i>	<b>8.0 ± 1.3</b>	<b>16.5 ± 7</b>	<b>27.7 ± 10.8</b>	<b>13 ± 2.6</b>

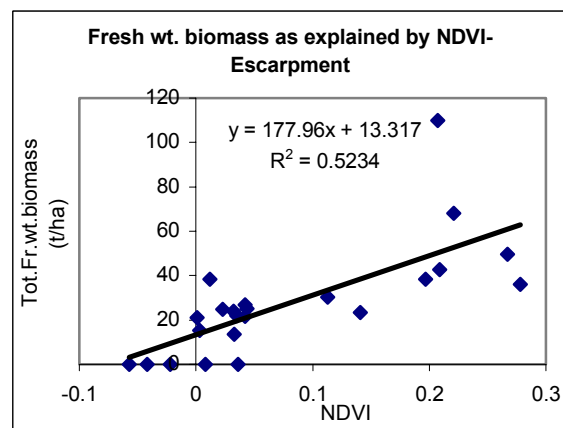
**Table 5.3: Stratified random sampling results for aboveground woody fresh weight biomasses.**

Results from a simple random sampling assumption gave a sample and estimated population mean of  $17 \pm 4.12$ , with a standard error of 2.15 and sampling error of 25.36%.

### 5.3. Tree Cover, NDVI and Fresh Biomass Relationships



$$r = 0.811443$$



$$r = 0.723462$$

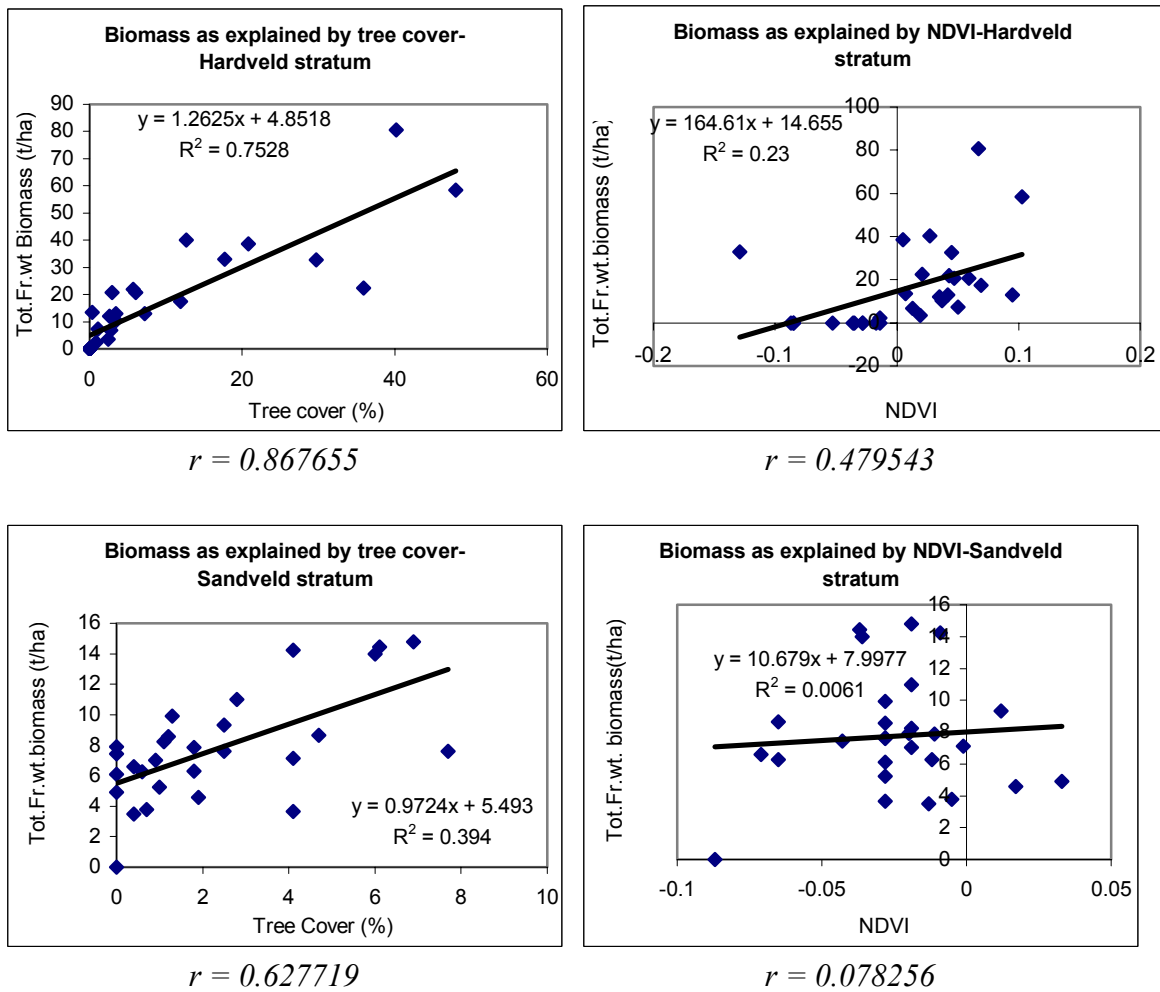


**Figure 5.7: Total aboveground fresh weight biomasses of each stratum as explained by tree cover and NDVI.**

For the entire sampling plots the graphs of tree cover and *NDVI* against aboveground fresh weight biomass is as shown below.

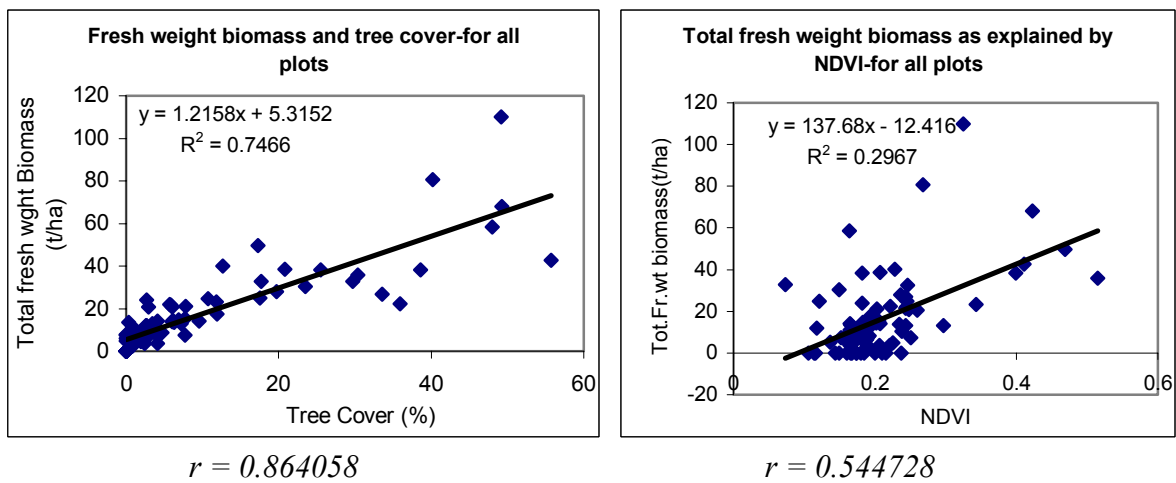


**Figure 5.8: Summaries of the relationships between total aboveground fresh weight biomass and total tree cover and NDVI for all the sampling plots.**

**5.4. Determinated Carbon Content in Serowe Species.**

The hypotheses and assumption under which this test was performed are stated in the previous chapter-sections 4.5.2 and 4.5.3 respectively.

Source of Variation	SS	df	MS	F	P-value	F <sub>crit</sub>
Between Species	68.9352	9	7.65947	21.934	8.206x10 <sup>-13</sup>	2.124
Within Species	13.968	40	0.3492			
<b>Total</b>	<b>82.9032</b>	<b>49</b>				

**Table 5.4: ANOVA of carbon content (%) in branch samples of tree and shrub species P = 0.05, N = 50.**

The average carbon content means for ten species were summarised as shown in figure 5.9.

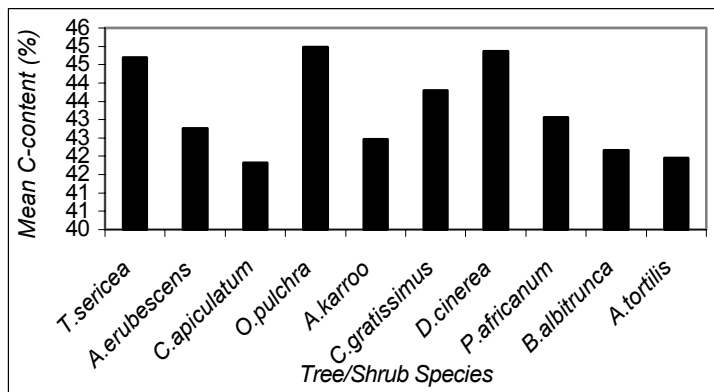


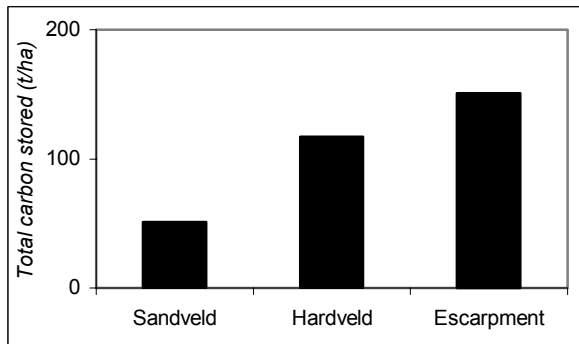
Table 5.5 below displays the two-tailed Student's t-test results for the ten tree/shrub species. The average carbon content in all the ten species was found to be a 0.43 ratio.

**Figure 5.9: Mean oven-dry carbon content per species; n = 5.**

Tree/Shrub Species	Test value = 0			Mean difference	95% Confidence Interval of the Difference	
	t	df	Sig.(2-tailed)		Lower	Upper
<i>Combretum apiculatum (a)</i>	100.720	4	.000	41.82	40.6672	42.9728
<i>Terminalia sericea (e)</i>	353.385	4	.000	44.70	44.3488	45.0512
<i>Acacia erubescens (ab)</i>	331.882	4	.000	42.76	42.4023	43.1177
<i>Acacia karroo (ab)</i>	147.737	4	.000	42.46	41.6620	43.2580
<i>Ochna pulchra (de)</i>	215.911	4	.000	44.98	44.4016	45.5584
<i>Croton gratissimus (cd)</i>	295.300	4	.000	43.80	43.3882	44.2118
<i>Dichrostachys cinerea (de)</i>	166.491	4	.000	44.86	44.1119	45.6081
<i>Boscia albitrunca (a)</i>	116.662	4	.000	42.16	41.1566	43.1634
<i>Acacia tortilis (a)</i>	120.826	4	.000	41.96	40.9958	42.9242
<i>Peltophorum africanum (abc)</i>	292.986	4	.000	43.06	42.6519	43.4681

**Table 5.5: Mean carbon content variance P = 0.05. Different letters in brackets for each species indicate significant difference-a ± standard error mean, N = 50, n = 5.**

### 5.4.1. Dry weight biomass and Carbon content



A fresh-dry weight biomass ratio (*FDBR*) of 0.5505 was used to convert fresh weight biomass into oven-dry weight biomass. The total amount of carbon in t/ha was thence computed from the oven-dry weight biomass using the above found average carbon ratio (0.43) in Serowe species.

**Figure: 5.10: Carbon sequestered totals in**

**each stratum,  $P = 0.05$ ; Sandveld =  $n = 27$ , Hardveld = 30 and escarpment = 23.**

### 5.4.2. Comparison of carbon content factors

The table below displays a comparison between results of two different carbon content ratios or factors. The 0.43 factor for Serowe has been derived from the findings of this study while the 0.5 factor is what is used mainly in the United States of America and in literature.

Stratum	Total fresh Weight Biomass (tons)	Total oven-dry weight biomass (tons)	Carbon Production/Content (tons)	
			Serowe (0.433)	United States of America (0.5)
Escarpment	630.70	347.2	150.34	173.60
Hardveld Acacia	468.12	257.7	111.58	128.85
Sandveld Savannah	216.62	119.25	51.63	59.63
<b>Total</b>	<b>1 315.44</b>	<b>724.15</b>	<b>313.56</b>	<b>362.08</b>

**Table 5.6: Stratum biomass and carbon amounts comparisons.**

### 5.5. The Vegetation and Carbon Maps

Having computed the *NDVI*, woody fresh weight biomass and carbon content from field measurements, the vegetation and carbon maps for the study area were generated. Results are as shown below:

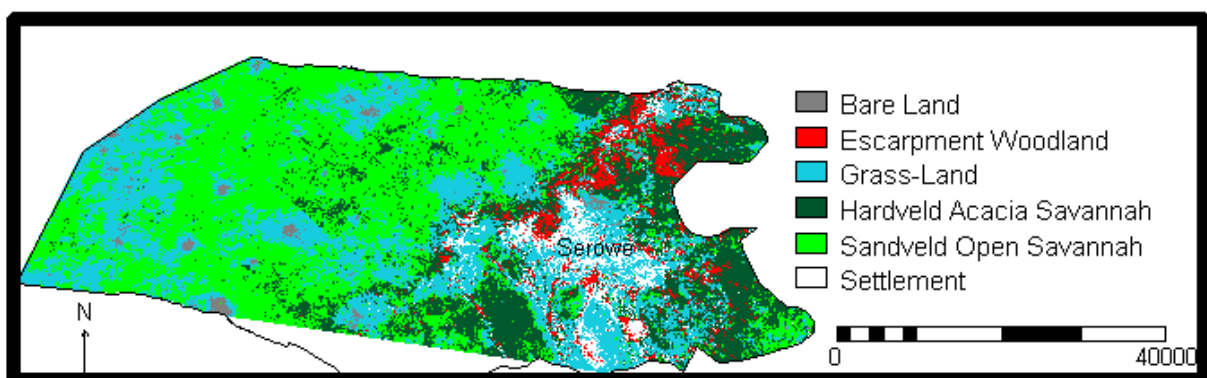


**Figure 5.11:** A vegetation map of Serowe. Note: Circular grey bare landmarks are cattle-posts or water wells abundant in the sandveld portion of the study area.

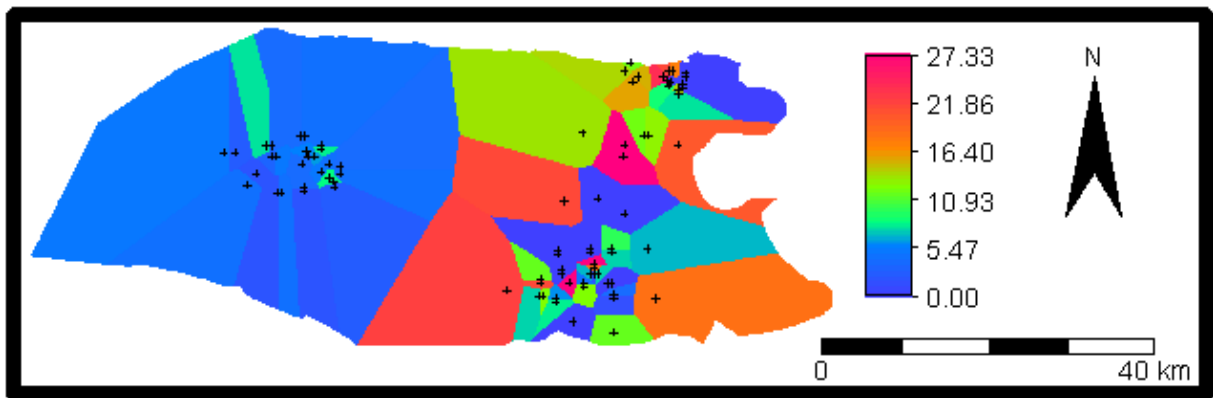


**Figure 5.12:** A carbon (t/ha) map for Serowe. The black-crosses (+) inside the map depict the location of the sampling plots.

#### 5.6. Biomass Estimation from Remote Sensing

An  $APAR$  ( $W/m^2$ ) map was generated as a product of the  $FPAR$  and  $K_d$  maps for input into the  $CASA$  algorithm. Note the similarity of this map to that of  $NDVI$ .

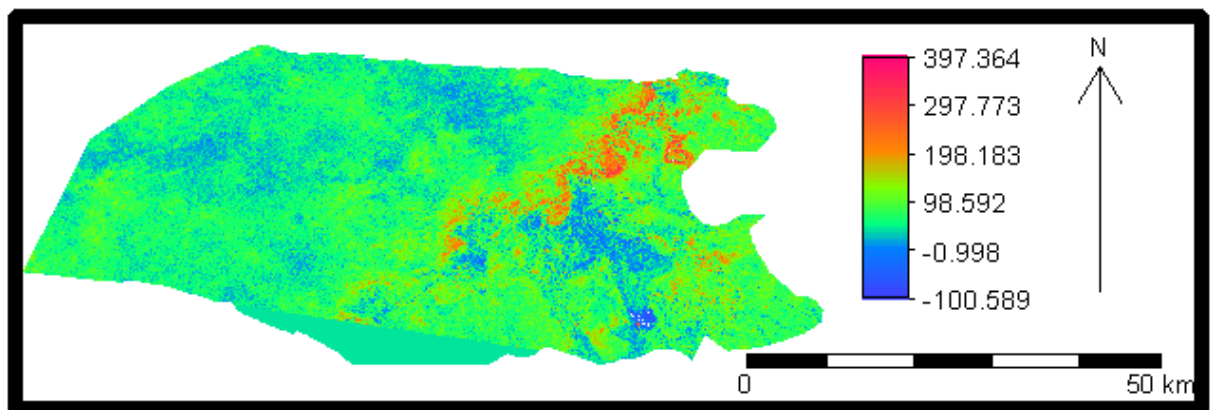


**Figure 5.13:**  $APAR$  ( $W/m^2$ ) map over the study area.

$NDVI$  and  $FPAR$  from the *Landsat-7 ETM+* of August 2000 images showed a strong relationship as displayed in the figure below:

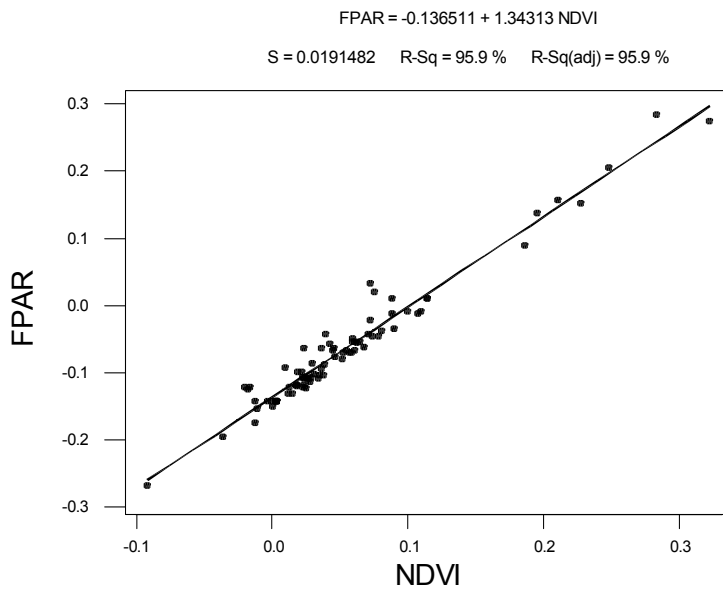


Figure 5.14: Relationship between FPAR as a function of NDVI.

### 5.6.1. Biomass/Carbon Estimates from Remote Sensing

Below is a graph showing the regression analysis of remotely obtained biomass values (*t/ha*) and the field oven dry weights of biomass (*t/ha*):

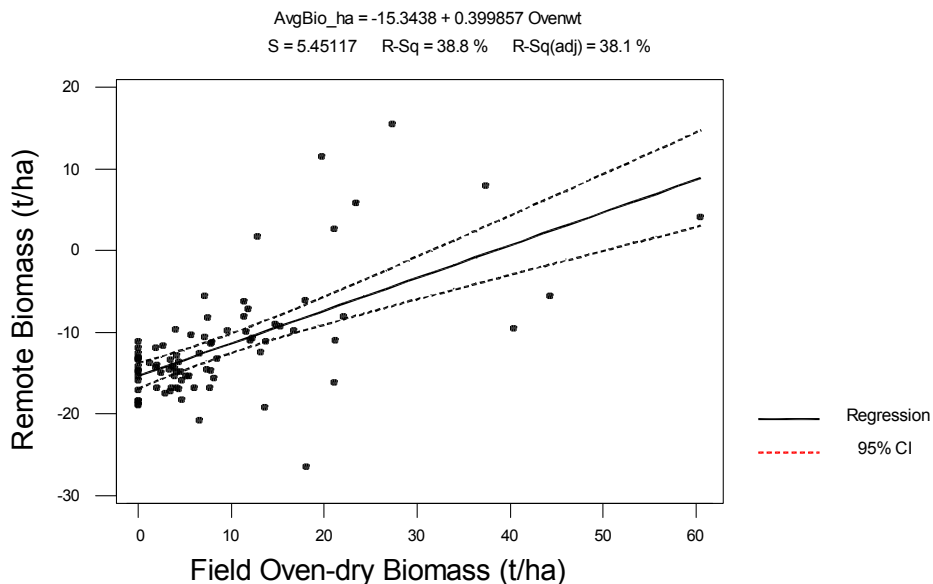


Figure 5.15: Remote biomass estimates as explained by field oven-dry total biomass.

### 5.7. Comparison of the Estimates from the Two Methods

Testing for a significant difference between the field based carbon estimate and the remotely sensed based carbon estimate, the two- tailed Student's t-test gave the following results:

---

#### Two-Sample T-Test and CI: C-ground estimate (Cgnd), C-remote estimate (RemoteC)

Two-sample T for Cgnd vs RemoteC

	N	Mean	StDev	SE Mean
Cgnd	83	3.89	4.64	0.51
RemoteC	83	-5.04	2.98	0.33

Difference = mu Cgnd - mu RemoteC  
 Estimate for difference: 8.930  
 95% CI for difference: (7.734, 10.127)  
 T-Test of difference = 0 (vs not =): T-Value = 14.76, P-Value = 0.000 DF = 139

---

**Table 5.7: Field carbon estimates versus remote carbon estimates.**

---

#### Regression Analysis: RemoteC versus Cgnd

The regression equation is: RemoteC = - 0.305 Cgnd

Predictor	Coef	SE Coef	T	P
Noconstant				
Cgnd	-0.3051	0.1017	-3.00	0.004

S = 5.585

Analysis of Variance

Source	DF	SS	MS	F	P
Regression	1	281.07	281.07	9.01	0.004
Residual Error	82	2557.71	31.19		
Total	83	2838.78			

Unusual Observations

Obs	Cgnd	RemoteC	Fit	SE Fit	Residual	St Resid
15	16.1	3.446	-4.910	1.636	8.356	1.56 X
55	19.1	-2.352	-5.819	1.938	3.467	0.66 X
56	11.8	6.671	-3.585	1.194	10.256	1.88 X
57	26.0	1.779	-7.946	2.647	9.725	1.98 X
65	17.4	-4.071	-5.309	1.769	1.239	0.23 X

X denotes an observation whose X value gives it large influence.

---

**Table 5.8: The regression analysis of remotely sensed and field measured carbon values.**

## 5.8. The Carbon Status in Serowe

### Descriptive Statistics: Cgnd

Variable	N	Mean	Median	TrMean	StDev	SE Mean
Cgnd	83	3.886	2.350	3.253	4.640	0.509
Variable	Minimum	Maximum	Q1	Q3		
Cgnd	0.000	26.040	0.890	5.300		

**Table 5.9: Statistics of sequestered carbon in Serowe.**

	Area (ha)	Mean Carbon Density (t/ha)	Total Carbon (tons)	Confidence Interval (tons/ha)
<b>Carbon Pool</b>	<b>244 047.6</b>	<b>3.8</b>	<b>927 381</b>	<b>± 0.62</b>

**Table 5.10: A summary of the carbon status (baseline carbon distribution) in Serowe.**

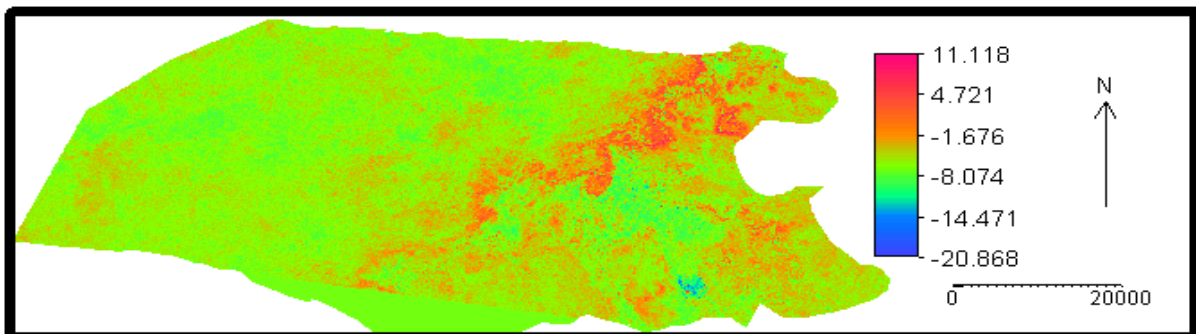


**Figure 5.16: Carbon sequestration estimates (t/ha) from remote sensing.**

## 6. DISCUSSION

### 6.1. Vegetation and the Serowe Environment.

A reconnaissance survey of the study area revealed that the study area's vegetation population is heterogeneous but homogeneous enough to allow stratification with respect to spatial distribution. This characteristic justified the division of the study area into three strata, namely the sandveld, hardveld and escarpment as showed in figure 5.2. The hardveld stratum statistically gave a very high sampling error before the outlier-sampling unit in sample plot 65 and the three plots that fell into the built-up area of Serowe village were removed.

The variation in the hardveld stratum is caused by the varied nature of the topography ranging from bare land to small river valleys. Here vegetation cover and land use include; grasslands, protected forests (Sokwe forest), dominant acacia communities, agricultural land portions, bigger settlements (including Serowe and Mogorosi), and dense riparian vegetation southwest of Serowe. As (Timmermans and Meijerink, 1999) reports, the soils and soil moisture conditions vary extensively. This causes a varied mixture of micro ecological settings inhabited by different plant communities.

Although the study area falls into a semi-arid climatic category, the escarpment band of vegetation mostly shows green dense vegetation both on top of the escarpment and the foot of it with tree canopy covers reaching a maximum of 56%. This result is relatively comparable with the estimates given by Timmermans and Meijerink. They gave a range of ratios of tree canopy cover of 10% to 60%. In this study a minimum percentage cover of 2.7% was computed. No convincing reason has been forwarded to explain the existence of this dense band of vegetation on the realms of the escarpment. (Ecosurv, 1997) in (Timmermans and Meijerink, 1999) postulate that the vegetation may be extracting soil water from a larger depth while Timmermans and Meijerink add that seasonal perched water tables may be playing a role in the distribution patterns of this vegetation.

Nonetheless, field surveys with a soil auger at the time of fieldwork in September/October, revealed that the soils have a great moisture storing capacity. In this semi-arid environment, it was surprising to find the soils very moist at a depth of ~5 cm four days after the first drizzles. It appears also that the combined large tree cover ratio contributes to the slow rate of water loss. Perhaps (Moll and Moll, 1994) give a more lucid answer in that the escarpment vegetation may be said to be afro-montane. Afro-montane forests are found on hills or mountains whose rocks have the ability to store seasonal rainfall water up to the next season. It was also noted during fieldwork that a number of tree species have special climatic adaptive features of which a good example is *Ricinodendron rautananii* (Mokong'wa). This tree exhibits low wood density characteristics and has a large trunk with water storing capacity.

The above points are relevant to this study in that as (Goward et al., 1985) report, the amount and type of vegetation cover influences moisture exchanges with the atmosphere. This is with respect to soil hydraulic properties, rooting characteristics, soil moisture status and atmospheric demand, in sustaining a supply of water at the evaporating surface (stomata).

It was also that the sandveld stratum showed the most homogeneity in vegetation type mostly shrubs of the *Acacia erubescens* (Mohahu/Moloto), *Terminalia sericea* (Mogonono), *Boscia albitrunca* (Motopi) and *Ochna pulchra* (Monyelenyele) species. Conversely, the Hardveld (plots 36 to 65) and Escarpment strata show a disparity within themselves where some

portions reflect a higher biomass accumulation in trees while other portions show high biomass values in shrubs.

### 6.1.1. Tree Cover and Biomass

Serowe is characterised by a semi-arid environment, which is dominated by the acacia tree and shrub species that are in themselves characterised by small, narrow needle-like leaves. Such leaves are difficult to detect from the satellites' elevation especially in an arid environment where the greenness of the vegetation is affected by limited water supply. Since the aboveground tree component accounts for the greatest fraction of total biomass density, and to a greater extent *NDVI*, tree canopy cover was found to explain about 75% of the aboveground fresh weight biomass in the entire study area. See figure 5.8.

The above value could be explained in the sense that in some sampling plots, biomass was recorded not from trees but from shrubs only. Therefore, the 25% remainder in this explanation of biomass can be attributed to shrub cover. This conforms to the *NDVI* map in that the *Landsat-7 ETM+* image (*August 11, 2000*) bands (543) false colour composite may not have reflected the true nature of the potential standing biomass items due to the asynchronous phenology (some species losing leaves while others are flushing them out) of many trees in tropical environments (WRI, 2001). In August, *Combretum apiculatum* (Mohudiri), *Dichrostachys cinerea* (Moselesele) and many other seemingly deciduous plants had shed their leaves hence giving a false impression of the *NDVI* and thence the biomass density from satellite observation. *Acacia erubescens* (Mohahu) was observed to have very small brownish-yellow coloured leaves, which may not well be sensed by the satellite sensors the implications of which are obvious in image biomass estimations.

### 6.1.2. NDVI as a Biomass Predictor

From table 5.2, it can be observed that the escarpment stratum has the greatest variance exhibiting the greatest heterogeneity. Field observations indeed reveal that in this stratum, one could find nearly all the tree and shrub species found both in the sandveld and hardveld strata. The vegetation varies from open grassland to dense woody bush land. The dense woodland was found on top of the escarpment and on particular escarpment faces. The tree canopy cover was calculated and found to vary between 0 to 56% with total fresh weight biomass ranging from 0 to 110 tons/ha.

Figures 5.7 and 5.8 show how tree canopy cover and *NDVI* explain the total aboveground fresh weight biomass in the respective strata and the entire study area respectively. In the escarpment, tree canopy cover explains 66% of the total aboveground fresh weight biomass while *NDVI* explains 52%. The results are as expected because the 66% cover is only attributed to trees and not shrubs. Thence one would be right to adduce that the shrub cover, which was not measured in this study, explains the other 34% of the biomass. For *NDVI*, both the spectral attributes of the trees and shrubs are catered for but the result is as is expected since some trees whose biomass was measured did not have some leaves. In addition, the acacia species had very small yellowish leaves, which may suggest that the satellite sensors never recorded the weak signal from such.

The high *NDVI* values on the *NDVI* map displays a band of red indicating the density of the vegetation. This is in line with the findings of many researchers including (Sellers, 1987) who observed that *NDVI* is an indicator of biomass. This is supported by the results in this study as

the escarpment stratum gave the highest value of biomass. See table 5.5. Hence, the use of *NDVI* as a remote sensing surrogate for leaf area index (*LAI*) is justifiable (Hartfield et al., 1984; Asrar et al., 1992 in (Bastiaanssen and Ali, 2001). (Sellers, 1987) further states that the time integral of the *APAR* as estimated from spectral reflectance of vegetated land surfaces was found to be near-linearly related to *NPP*. Although *NDVI* is a good estimator of rates associated with vegetation (photosynthesis, transpiration), it is an unreliable indicator of the state of the vegetation (*LAI*, Biomass) - (Sellers, 1985 in (Sellers, 1987). This observation marches the relationships observed for the hardveld and sandveld total fresh weight biomass as explained by *NDVI*.

This weakness of *NDVI* in depicting aboveground dry matter biomass (Tucker, 1979); (Christensen and Goudriaan, 1993) and (WRI, 2001)) is the reason why the *PAR* approach in biomass and carbon estimations from remotely sensed data is preferred. In Serowe, this weakness of *NDVI* in predicting biomass is exacerbated by the dry climate and the asynchronous phenology of the vegetation found therein. Thence, *SEBAL*, which is less dependent on *NDVI*, was found to be an appropriate method.

Nonetheless, *NDVI* is essential in mapping land cover as it was used in the generation of the vegetation map shown in figure 5.11. The accuracy of the classification was not assessed due to time limitations. It is also an essential input for the calculations of *FPAR*,  $G_o$  and  $\epsilon_o$ . Due to the asynchronous phenology in the study area, the month with the maximum *NDVI* was assumed to be February, which falls within the rain season, an assumption that was used in the determination of  $T_1$  and  $T_2$  in the *CASA* model.

## 6.2. Field/Remote Measurements of Biomass

Since the amount of carbon stored in a given area is simply a ratio of the amount of biomass found in that area, the study of biomass quantities gives an estimate of the amount of carbon. Results obtained from field measurements of biomass derived from allometric equations portray the reality in the field. See table 5.6. These results were obtained at  $P = 0.05$  with a margin of error of not greater than 0.51 being unacceptable as it was already pre-calculated as explained in chapter four.

For remote sensing, the use of the *PAR* related method gave the results as displayed in table 5.6. As the results are dependent on the water-energy relationships as explained in chapter two, the total accumulated dry matter appears to be in line with the field measurements.

The evaporative fraction (0.2801) was found not to conform with the findings of (Timmermans and Meijerink, 1999) who applied *SEBAL* to groundwater management studies yielding actual evapotranspiration (*Ea*) rates of 1.5 – 3 mm/day. The less vegetative cover, the less the latent heat losses and thence the higher the surface temperature. This is so because there is less or no water to dissipate the incoming solar energy. It is also decipherable from the graph that the sandveld stratum shows the most homogeneity in vegetation type mostly shrubs of the *Acacia erubescens* (Mohahu/Moloto), *Terminalia sericea* (Mogonono), *Boscia albitrunca* (Motopi) and *Ochna pulchra* (Monyelenyele) species. Conversely, the hardveld (plots 36 to 65) and Escarpment strata show a disparity within themselves where some portions reflect a higher biomass accumulation in trees while other portions show high biomass values in shrubs.

The mean parameter of the entire population was calculated to be  $13 \pm 2.6$  t/ha aboveground fresh weight biomass. The results show that the escarpment vegetation has the largest stocks of carbon (sum of 150 tons) while the sandveld has the lowest sum of 52.

### 6.3. The Serowe Carbon Conversion Factor

In literature, the *0.5-factor* is loosely used. It is sometimes used to directly convert fresh weight biomass to organic carbon weight (MacDicken, 1997); (Brown, 1997) while others use it to convert fresh weight biomass to dry weight biomass. In this study, a specifically obtained fresh-dry weight conversion factor (*0.6*) was used. Studies conducted by De Gier (lecture notes) and (Kabore, 1991) indicate that total dry weight is always higher than half the weight of fresh weight biomass. Then a Serowe determined oven-dry weight biomass conversion factor of *0.43* to carbon was employed. These factors are within the range of values found in literature. For instance, (Kilawe et al., 2001) used a carbon conversion factor of *0.45* in Tanzania. (MacDicken, 1997) applies a ratio of *0.5* in his carbon estimation manual. These factors apparently standard out to be close to one another and the chemically computable carbon ratio in nominal dry weight matter (wood)-( $C_6H_9O_4$ ), as given by Washington University's educational website (Washington, 1997). From this chemical formula, the percentage of carbon would be computed as:

$$C_6H_9O_4 = (12*6) + (1*9) + (16*4) = 145 \text{ grams}$$

$$\therefore \% \text{ Carbon: } 72/145*100 = \underline{49.655 \%}$$

However, the above nominal dry wood ratio includes the carbon weights from oils, sugars and resins.

From table (5.4), it is clear that there is a significant difference in the means of the ten species suggesting that there is a significant statistical difference in carbon contents in these species with  $P < 8.206E-13$ . Thus, mean carbon content in woody plants is dependent on species type. To effectively explain the source of these differences among the species' oven-dry carbon content means, the *coefficient of determination (R-Square)*-was computed (Moore and McCabe, 1999). The resultant value of *0.8315* tells us that the differences among the means of the species, accounts for 83.2% of the total variation in the species' oven-dry carbon content results. However, the computed weighted mean oven-dry conversion factor of dry weight biomass to carbon was found to be *0.43*-a value used to convert biomass to carbon in this study.

In remotely sensed data however, only one conversion factor (i.e., one that converts dry weight biomass to carbon amounts) since the derived biomass values give a dry weight status, would be necessary.

In Serowe Botswana, *Dichrostachys cinerea* (Moselesele), one of the most dominant species forms vast clusters of itself (in shrub form) with a few other species in this semi-arid environment. Although very few tree forms of this species were found at the time of the survey, laboratory results suggest that the species together with *Ochna pulchra* (Monyelenyele) have the largest carbon content. In comparison to Moselesele, Monyelenyele is scantily scattered mostly in the sandveld.

The third largest storer of carbon is *Terminalia sericea* (Mogono), a species that was found to be balanced in forms of its existence. In the sandveld, its predominant as a shrub but occurs as young trees in the escarpment woodland. *Combretum apiculatum* (Mohudiri), was found mainly in tree form and dominating all the tree species found in Sokwe forest south of Serowe village. The average carbon storage of this species was found to be 42% a value that is ranking ninth out of the ten species analysed by the Dumas-method in descending order of all the organic carbon content means.

#### 6.4. Comparisons Between Field and Remote Measurements

The two tailed Students' t-test suggested that there is a difference between the carbon means obtained from remotely sensed data and that obtained from field estimation. Surprisingly, the mean carbon value from remotely sensed data gave a negative value. The explanation for this is a compound of possible reasons including the calculation of the aerodynamic resistance ( $r_{ah}$ ), which is very complicated to calculate. Reginato et al., (1985) allude to the large errors in the determination of sensible heat ( $H$ ) to the errors in the measurements (or extrapolation) of air temperature whose standard elevation level of measurement is 2 m. In the field air temperatures were only obtained from the sandveld stratum. Due to the large variance in the vegetation height, the determination of the displacement height ( $d$ ) may introduce errors. This was compounded by lack of LAI data hence the use of the average tree cover ratio. Since these parameters are inputs in the determination of 'Z<sub>o</sub>', accurate values or estimates are crucial for the accurate estimation of the evaporative fraction (Reginato et al., 1985).

The analysis of variance shown that 38% (adjusted coefficient of determination) of the carbon estimates on the ground can be explained by remotely sensed data. The analysis reveals that there must have been a lot of errors on the calculation of carbon from remotely sensed data. Table 5.8 displays the regression analysis results showing the five sampling plots where the large errors emanated from. Three of these plots are from the escarpment woodland stratum while two are from the hardveld stratum. Plot 55 in the hardveld is a protected woodland (Sokwe forest) while plot 65 exists on the riverine woodland. Lack of meteorological parameters data for these areas may have contributed to the negative records of carbon estimates from remotely sensed data. Since *NDVI* is used as a surrogate of *LAI* in the calculation of *FPAR*, low to negative values of *NDVI* measurements in these areas may have caused the significant difference.

The hardveld stratum is located mainly on darker soils. This compounded by the small leaves on relatively large acacia trees reduced the  $r_o$ . In the escarpment stratum, large trees were found in plots 15 and 56 whose canopies had no leaves. This contributes to high biomass values for ground-determined estimates with little effect on satellite recordings. However, the actual causes of the negative values in the remotely sensed data set in this study have not been known.

Generally, as local conditions play a crucial role in any given area's capabilities to store carbon, methods that embrace the variability of the landscape and climatic conditions such as the method followed in this study should be preferred. The approach encourages the production of spatial and temporal map products that are very important in carbon management in comparison to landuse, land-use change and forestry. Because of their relatively ease in interpretation, maps will play a crucial role when carbon becomes an internationally tradable commodity.

## 7. CONCLUSIONS & RECOMMENDATIONS

### 7.1. Study Outputs

The study has shown that estimates of biomass and carbon from remotely sensed data are feasible. In addition, the inherent map production characteristics of the approach provide an easy way of analysing outputs over a large area in a one-time investment. This study has produced some baseline data and information regarding the status of the organic carbon stocks in Serowe. Furthermore, the study has produced an oven-dry weight biomass to carbon amounts conversion factor of *0.43* specific to the study area but with potential to be used in other semi-arid areas in the Southern African region. The net carbon sequestered in Serowe has been found to be *752 000* tonnes on an area of *244 048* hectares.

#### 7.1.1. Conclusions

Based on the results obtained, the following conclusions are drawn:

- ◆ that the accuracy of estimating carbon sequestered in aboveground woody biomass from remotely sensed data with the use of *SEBAL* and *CASA* algorithms is not precise and efficient.
- ◆ although carbon sequestration has been found to be species dependent, a general average factor can be derived for the purposes of converting oven-dry weight biomass to carbon quantities. In Serowe this factor has been determined to *0.43*.
- ◆ that in the semi arid environment, spectral reflectance data and tree cover are unreliable indicators of the state of fresh weight aboveground biomass. They are also not reliable inputs in the algorithms for the estimation of carbon due to asynchronous phenology of the vegetation.

#### 7.1.2. Recommendations

- ☉ More experimental research is recommended in the verification and establishment of the empirical relationships between the Water-Energy-Carbon Labyrinth in order to strengthen and validate the use of such relationships in different environmental settings. This will render the use of remote sensing and *GIS* in carbon sequestration a powerful and reliable tool. Such research areas include studies on *LAI* in semi-arid environments and the savannah in general and the effects of the asynchronous phenology behaviour of the vegetation.
- ☉ In the acquisition of climatic variables, this study recommends that two to three *20* to *25 m* weather towers for the recording of gas and energy fluxes if built in the region would act as control or standard reference points not only in carbon sequestration studies but also in climatological, agro-meteorological hydrological and ecological studies. Relatively spread out ground stations for the measurements of  $K_d$ , air temperature ( $T_a$ ) and wind speed ( $u$ ) can tremendously improve the accuracy of calculating actual evapotranspiration with special attention to the calculation of the aerodynamic resistance to heat transfer.

### 7.2. Application of Research

The research's results may act as a baseline-information for future studies, planning and management of land and carbon budgets in Serowe-Botswana. It may contribute to the development of further sound management strategies of the study area considering the fact that it is an animal husbandry area. Apart from the potential use in carbon sequestration, the

methodical procedure may also be used as a stimulant for further research in ecology and meteorology.

Most of all, the approach of incorporating *SEBAL* and *CASA* may prove to be a powerful but relatively cheaper method for use under the Kyoto Protocol as carbon management (sequestration and monitoring) becomes an international trade through the implementation of the Clean Development Mechanisms (*CDMs*), new afforestation projects and the already existing Joint-Implementation (*JI*)-Projects. This approach, involving the aspects of GIS and remote sensing, has the capability of being used as a regional, national or global scale carbon sequestration measuring and monitoring tool.

## REFERENCES:

- Bastiaanssen, W.G.M., and S. Ali. 2001. A New Crop Yield Forecasting Model Based on Satellite Measurements Applied Across the Indus Basin, Pakistan. Submitted to Agriculture, Ecosystems & Environment:24.
- Bastiaanssen, W.G.M., M. Menenti, R.A. Feddes, and A.A.M. Holtslag. 1998. A Remote Sensing Surface Energy Balance Algorithm for Land-1-formulation. Journal of Hydrology 212-213:198-212.
- Brown, S. 1997. Estimating Biomass and Biomass Change of Tropical Forests-A Primer FAO, Rome-Italy.
- Brutsaert, W. 1982. Evaporation into the Atmosphere-Theory, History and Applications. D. Reidel Publishing Company, Dordrecht, Holland.
- Christensen, S., and J. Goudriaan. 1993. Deriving Light Interception and Biomass from Spectral Reflection ratio. Remote Sensing Environment 48:87-95.
- Costa, P.M. 1996. Tropical Forestry Practices for Carbon Sequestration: A Review and Case Study from Southeast Asia. Ambio 25:279-278.
- Daughtry, C.S.T., K.P. Gallo, S.N. Goward, S.D. Prince, and W.P. Kustas. 1992. Spectral Estimates of Absorbed Radiation and Phytomass Production in Corn and Soybean Canopies. Remote Sensing of Environment 39:141-152.
- Davis, K.J., A.S. Denning, and P.S. Bakwin. 2000. Quantifying North American Sources and Sinks of CO<sub>2</sub> via Synthesis of in Situ Data, Remote Sensing and Inverse Modeling. Research Proposal 00-OES-08. The Pennsylvania State University, Pennsylvania.
- Dingman, S.L. 1994. Physical Hydrology Prentice Hall, Inc., New Jersey 07458.
- DOE. 2001. Carbon Sequestration in Terrestrial Ecosystems [Online]. Available by CSiTE <http://csite.esd.ornl.gov/index.html> (posted April 26, 2001; verified July 12, 2001).
- Ecosurv. 1998. Vegetation Mapping and Ground Truthing for Radar Imagery. Descriptive Report. Ecosurv.
- FAO. 2001. State of the World's Forests-2001 FAO-Information Division, Viale delle terme di Caracalla, 00100, Rome, Italy.
- Field, C.B., J.T. Randerson, and C.M. Malmstrom. 1995. Global Net Primary Production: Combining Ecology and Remote Sensing. Remote Sensing and Environment 51:74-88.
- Frouin, R., and R.T. Pinker. 1995. Estimating Photosynthetically Active Radiation (PAR) at the Earth's Surface from Satellite Observations. Remote Sensing and Environment 51:98-107.
- Goward et al. 1985. Observed Remote Sensing of Environment Relation Between Thermal Emission and Reflected Spectral Radiance of a Complex Vegetated Landscape. Remote Sensing Environment 18:137-146.
- Houghton, R.A. 1996. Converting Terrestrial Ecosystems from Sources to Sinks of Carbon. Ambio 25:267-272.
- IPCC. 2000. Land Use, Land-Use Change and Forestry; - A special report of the Intergovernmental Panel on Climate Change (IPCC) Cambridge University Press, The Edinburgh Building, UK.
- Kabore, C. 1991. Biomass. MSc., International Institute for geo-Information and Earth Observation (ITC), Enschede-The Netherlands.
- Kilawe, E.C., L.P. Lusambo, J.H.Y. Katima, S. Augustino, N.O. Swalehe, B. Lyimo, and S. Luwagila. 2001. Aboveground biomass equations for determination of carbon storage in plantation forests in Kilombero District, Mgorogoro-Tanzania. International Forestry Review 3.

- Lange O. L., Nobel P. S., Osmond C. B., and Ziegler H., (eds.) 1982. Physiological Plant Ecology II-Water relations and Carbon Assimilation, Vol. 12B, pp. 1-747. Springer-Verlag, Wurzburg/Berlin.
- Lemenih, M. 1995. Woody Biomass Assessment of Trees and Shrubs for Fuelwood in Ziway region Woodland, Ethiopia. MSc-Thesis, ITC, Enschede.
- Lillesand, T.M., and R.W. Kiefer. 2000. Remote Sensing and Image Interpretation. 4th ed. John Wiley & Sons, Inc., New York.
- MacDicken, K.G. 1997. A Guide to Monitoring Carbon Storage in Forestry and Agroforestry Projects. Winrock International Institute for Agricultural Development., USA.
- Matejovic, I. 1996. The Application of Dumas Method for determination of Carbon, Nitrogen and Sulphur in Plant Samples. Rostlinna Vyroba 7:313-316.
- Moldenhauer, O., and M.K.B. Lüdeke. 2000. Climate Sensitivity of Global Terrestrial Net Primary Production (NPP) Calculated using the Reduced Form Model-NNN. Potsdam Institute for Climate Impact Research, D-14412, Germany, Potsdam.
- Moll, E., and G. Moll. 1994. Struik Pocket Guide-Common trees of Southern Africa Struik Publishers (Pty), Cornelis Struik House, 80 McKenzie Street,, Cape Town-South Africa.
- Moore, D.S., and G.P. McCabe. 1999. Introduction to the Practice of Statistics. 3rd ed. W. H. Freeman & Company, New York.
- NASA. 2001. NASA Facts Sheets [Online]. Available by NASA [http://pao.gsfc.nasa.gov/gsf/service/gallery/fact\\_sheets/earthsci/warming.htm](http://pao.gsfc.nasa.gov/gsf/service/gallery/fact_sheets/earthsci/warming.htm) (verified July 3).
- NTSG. 2002. Remote sensing of Net Primary Production [Online]. Available by Numerical Terradynamic Simulation Group-University of Montana-School of Forestry <http://www.forestry.umt.edu/ntsg/> (verified February 17).
- Obakeng, O.T. 2000. Groundwater Recharge and Vulnerability-A case study of the SE central Kalahari sub-basin, Serowe Region, Botswana. MSc., ITC-The Netherlands, Enschede.
- Palgrave, C.K. 1993. Trees of Southern Africa Struik Publishers, Cape Town-Republic of South Africa.
- Reginato, R.J., R.D. Jackson, and P.J. Pinter. 1985. Evapotranspiration Calculated from Remote Multispectral and Ground Station Meteorological Data. Remote Sensing Environment 18:75.
- Richardson, J., J.H. Everitt, and H.W. Gausman. 1983. Radiometric Estimation of Biomass and N-Content of Alicia Grass. Remote Sensing Environment. 13:179-184.
- Samarasingha. 2000. Vegetation Growth and Water Response Slide Show, Sri-Lanka.
- Sellers, P.J. 1987. Canopy Reflectance, Photosynthesis and Transpiration II-The role of biophysics in the linearity of their interdependence. Remote Sensing Environment 21:143-183.
- Sellers, P.J., B.W. Meeson, F.G. Hall, G. Asrar, R.E. Murphy, R.A. Schiffer, F.P. Bretherton, R.E. Dickinson, D.G. Ellingson, C.B. Field, K.F. Huemmrich, C.O. Justice, J.M. Melack, N.T. Roulet, D.S. Schimel, and P.D. try. 1995. Remote Sensing of the Land Surface for Studies of Global Change: Models-Algorithms-Experiments. Remote Sensing and Environment 51:3-26.
- Sumner, M.E., (ed.) 2000. Hand Book of Soil Science, pp. 1-A-1 - I-33. CRC Press, New York-United State of America.
- Tietema, T. 1993. Biomass Determination of Fuelwood Trees and Bushes of Botswana, Southern Africa. Forest Ecology and Management 60:257-269.
- Timmermans, W.J., and A.M.J. Meijerink. 1999. Remotely Sensed Actual Evapotranspiration: Implications for Groundwater Management in Botswana. JAG 1.

- Tucker, C.J. 1979. Red and Photographic Infrared Linear Combinations for Monitoring Vegetation. Elsevier North Holland Inc. 8:127-150.
- Tucker, C.J., C. Vanpraet, E. Boerwinkel, and A. Gaston. 1983. Satellite Remote Sensing of Total Dry Matter Production in the Senegalese Sahel. *Remote Sensing Environment* 13:461-474.
- Umich. 2001. educational website [Online]. Available by University of Michigan [http://www.sprl.umich.edu/GCL/paper\\_to\\_html/energyflow.html](http://www.sprl.umich.edu/GCL/paper_to_html/energyflow.html) (verified December 11).
- UNFCCC. 1997. Kyoto Protocol to the United Nations Framework Convention on Climate Change [Online]. Available by UNFCCC <http://www.unfccc.de/resource/docs/convkp/kpeng.html> (verified April, 26).
- Washington, U.o. 1997. Energy and Environment 1 [Online]. Available by University of Washington <http://www.me.washington.edu/~malte/engr341/index.html> (verified June 12,).
- White, J. 2001. The Link Between Carbon and Water. Joseph White's Website- [http://www.baylor.edu/~Joseph\\_D\\_White/](http://www.baylor.edu/~Joseph_D_White/), Baylor-Waco USA.
- WRI. 2001. Remote Sensing Technology for Vegetation Monitoring [Online]. Available by World Resources Institute (WRI) <http://www.wri.org/press/co2comm.html> (posted October 8; verified November, 12 2001).
- Xiao, X., J.M. Melillo, D.W. Kicklighter, Y. Pan, A.D. McGuire, and J. Helfrich. 2001. Net Primary Production of Terrestrial Ecosystems in China and its Equilibrium Responses to Changes in Climate and Atmospheric CO<sub>2</sub> Concentration [Online]. Available by *Acta Phytocologica Sinica* (verified 27th December).

## APPENDICES

### APPENDIX AI: Names of tree/shrub species investigated and found in the study area.

No.	Setswana	English	Scientific
1	Mhata/Mohata	<i>Kalahari Apple-leaf</i>	<i>Lonchocarpus nelsii</i>
2	Mmaba	<i>Violet tree</i>	<i>Securidaca longependunculata</i>
3	Modubatsipi	<i>(Combretaceae)</i>	<i>Combretum molle. Br. Ex G. Don</i>
4	Modumela	<i>False Marula</i>	<i>Kirkia acuminata/Lannea schweinfurthii</i>
5	Motsiara	<i>(Combretaceae)</i>	<i>Terminalia prinioides</i>
6	Mogonono	<i>Silver Cluster-leaf</i>	<i>Terminalia sericea</i>
7	Mogorogorwane	<i>Corky-Bark Monkey Orange</i>	<i>Strychnos cocculoides</i>
8	Mogotho	<i>Camelthorn</i>	<i>Acacia erioloba</i>
9	Mohahu/Moloto	<i>Blue Thorn</i>	<i>Acacia erubescens</i>
10	Mohudiri	<i>Bushwillow, Red</i>	<i>Combretum apiculatum</i>
11	Mokabi	<i>Bushwillow, Russet</i>	<i>Combretum hereroense</i>
12	Mokgalo	<i>Buffalo-thorn</i>	<i>Ziziphus mucronata</i>
13	Mokhi	<i>Common Hook-thorn</i>	<i>Acacia caffra</i>
14	Mokoba	<i>Knob-thorn</i>	<i>Acacia nigrescens</i>
15	Mokongwa/Mongongo	<i>Manketti</i>	<i>Ricinodendron rautananii</i>
16	Moku	<i>Ana Tree</i>	<i>Acacia albida</i>
17	Monato	<i>Wild Syringa</i>	<i>Burkea africana</i>
18	Mongana		<i>Acacia mellifera</i>
19	Monyelenyele	<i>Peeling Bark Ochna</i>	<i>Ochna pulchra</i>
20	Moologa	<i>Lavender Feverberry</i>	<i>Croton gratissimus</i>
21	Mooka	<i>Sweet Thorn</i>	<i>Acacia karroo/A. Luederitzii</i>
22	Morutlwa		<i>Rothmannia capensis (Rubiaceae)</i>
23	Morutlhatshana	<i>(Thunb.)-Willd</i>	<i>Acacia caffra (Fabaceae)</i>
24	Moselesele	<i>Sicklebush</i>	<i>Dichrostachys cinerea</i>
25	Mosetlha	<i>Weeping Wattle</i>	<i>Peltophorum africanum</i>
26	Mosu/Mozu	<i>Umbrella Thorn</i>	<i>Acacia tortilis</i>
27	Motopi	<i>Shepherd's Tree</i>	<i>Boscia albitrunca</i>
28	Seroka		<i>Commiphora spp.</i>

### APPENDIX AII: Summary of 14 tree regression formulae for 14 most common species in Botswana; copied and modified from (Tietema, 1993).

Species	Setswana name	Regression Formula	n	R <sup>2</sup>	A. Code
<i>Acacia erioloba</i>	Mogotho	$B = 0.1376 \times BA^{1.2562}$	27	0.96	--
<i>Acacia erubescens</i>	Mohahu	$B = 0.1507 \times BA^{1.2647}$	88	0.94	MOH
<i>Acacia karoo</i>	Mooka	$B = 0.2865 \times BA^{1.2082}$	36	0.96	MOK
<i>Acacia luederitzii</i>	Mooka	$B = 0.1505 \times BA^{1.2835}$	19	0.90	--
<i>Acacia tortilis</i>	Mozu	$B = 0.1975 \times BA^{1.1859}$	109	0.93	MOZ
<i>Boscia albitrunca</i>	Motopi	$B = 0.2683 \times BA^{1.0455}$	23	0.93	MOT
<i>Combretum. apiculatum</i>	Mohudiri	$B = 0.2232 \times BA^{1.1001}$	58	0.85	MHU
<i>Croton gratissimus</i>	Moologa	$B = 0.0740 \times BA^{1.2668}$	34	0.97	MOO
<i>Dicrostachys. cinerea</i>	Moselesele	$B = 0.2787 \times BA^{1.0337}$	33	0.85	MOS
<i>Lonchocarpus nelsii</i>	Mohata	$B = 0.1936 \times BA^{1.1654}$	512	0.92	--
<i>Ochna pulchra</i>	Monyelenyele	$B = 0.1936 \times BA^{1.1654}$	512	0.92	MON
<i>Peltophorum africanum</i>	Mosetlha	$B = 0.1936 \times BA^{1.1654}$	512	0.92	MST
<i>Terminalia sericea</i>	Mogonono	$B = 0.0871 \times BA^{1.2286}$	12	0.95	MOG
<i>Ziziphus mucronata</i>	Mokgalo	$B = 0.2772 \times BA^{0.8914}$	30	0.80	--
<i>Combi-line</i>		$B = 0.1936 \times BA^{1.1654}$	512	0.92	--

**APPENDIX AIII:** Oven-dry total carbon content laboratory results of *the 50* samples from the ten common tree/shrub species in Serowe. Method of analysis: Dumas (*CNS-2000*-Analyser). Laboratory: Forestry and Forest Products Research Centre (*CSIR*)-South Africa, Nov 2001.

Species		Total Carbon Content (%)/Species					
Local Name	Scientific Name	Sample ID	Sample 1	Sample 2	Sample 3	Sample 4	Sample 5
Mogonono	<i>Terminalia sericea</i>	MOG	44.6	45.0	44.4	44.5	45.0
Mohahu	<i>Acacia erubescens</i>	MOH	42.8	42.4	42.7	42.7	43.2
Mohudiri	<i>Combretum apiculatum</i>	MHU	42.8	41.4	41.6	40.6	42.7
Monyeleneyele	<i>Ochna pulchra</i>	MON	45.0	45.5	44.3	45.3	44.8
Mooka	<i>Acacia karroo</i>	MOK	41.9	41.9	42.3	42.8	43.4
Moologa	<i>Croton gratissimus</i>	MOO	44.3	43.5	43.5	43.9	43.8
Moselesele	<i>Dichrostachys cinerea</i>	MOS	44.7	45.3	45.0	43.9	45.4
Mosetlha	<i>Peltophorum africanum</i>	MST	42.5	43.1	43.3	43.3	43.1
Motopi	<i>Boscia albitrunca</i>	MOT	43.0	42.5	42.7	41.4	41.2
Moza	<i>Acacia tortilis</i>	MOZ	41.2	42.4	41.6	43.1	41.5

**APPENDIX AIV:** Field data estimates of tree fresh weight biomass (*Tot. Fr.wt*), shrub fresh weight biomass (*Sh.Fr.wt*), total fresh weight biomass (*Tot.bio*) and the oven-dry weight (*Dr.wt.bio*). these values are expressed in (*t/ha*).

SamPlt #	X-Codes	Y-Codes	$n_i$	Tot.Fr.wt	Sh.Fr.wt	Tot.bio	NDVI	Dr.wt.bio
1	457165	7513373	12	29.379	10.769	40.149	0.043	22.102
2	435823	7526898	23	11.978	2.800	14.778	0.008	8.135
3	436303	7526520	30	4.899	9.540	14.439	0.015	7.948
4	434887	7527630	5	1.500	7.840	9.340	-0.010	5.142
5	434983	7527778	10	1.293	6.304	7.597	-0.016	4.182
6	477743	7530715	22	21.204	14.716	35.920	0.090	19.774
7	474097	7531855	12	5.653	15.512	21.165	0.079	11.651
8	473596	7531856	37	12.324	10.948	23.272	0.088	12.811
9	477815	7536765	15	11.723	1.924	13.647	0.085	7.513
10	477820	7537269	16	24.153	0.620	24.773	0.055	13.637
15	476271	7538927	41	39.623	28.348	67.971	0.112	37.418
16	475776	7538934	87	35.872	6.840	42.712	0.125	23.513
18	476430	7537879	27	10.456	4.904	15.360	0.089	8.456
19	476969	7539588	57	27.184	3.168	30.352	0.083	16.709
20	476462	7539574	93	29.279	9.040	38.319	0.088	21.095
21	472851	7538822	68	18.689	8.224	26.913	0.073	14.815
22	472346	7538821	60	20.399	7.424	27.823	0.090	15.317
23	472251	7540805	37	14.660	10.312	24.972	0.014	13.747
24	472264	7541280	19	7.906	13.648	21.554	0.047	11.866
31	469755	7517829	20	9.256	3.768	13.024	0.013	7.170
32	469734	7518329	31	14.954	2.460	17.414	-0.005	9.587
35	469960	7512400	2	2.273	0.000	2.273	0.060	1.251
36	469959	7512900	7	6.755	0.000	6.755	0.015	3.718
37	469959	7512900	16	5.892	16.060	21.952	0.015	12.085
38	466378	7514285	7	0.805	6.556	7.361	-0.002	4.052
39	467080	7515230	10	3.040	8.936	11.976	0.028	6.593

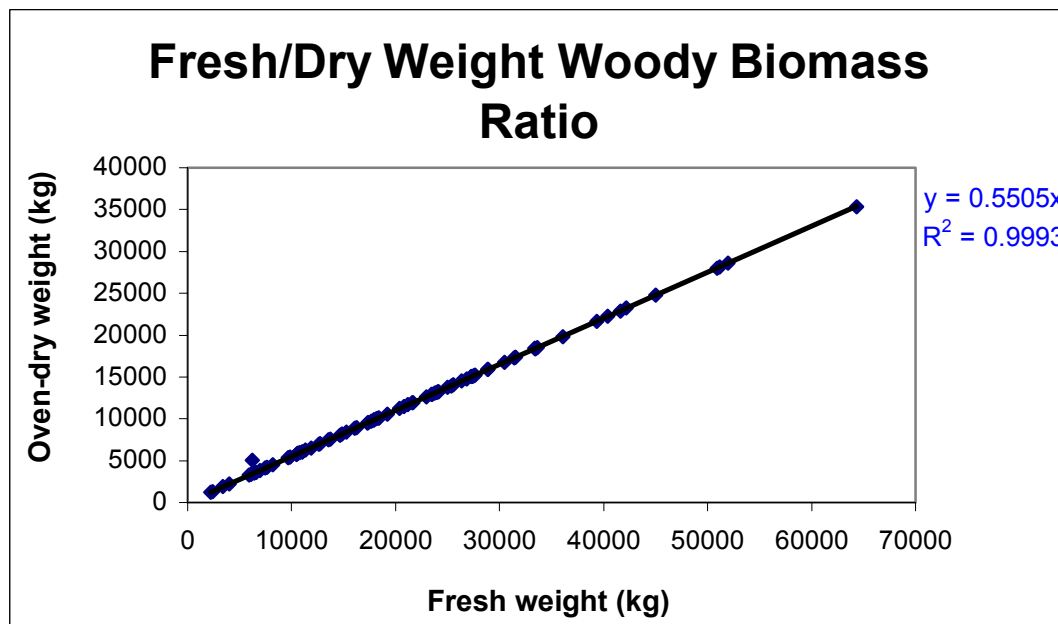
40	467580	7515246	4	2.482	1.012	3.494	0.015	1.924
41	468070	7515760	27	0.536	12.928	13.464	0.008	7.412
42	461227	7514672	11	3.228	17.396	20.624	0.016	11.354
43	461233	7514166	44	31.875	6.664	38.539	0.029	21.216
44	460890	7512597	21	5.050	7.996	13.046	0.020	7.182
45	461389	7512596	28	11.840	10.544	22.384	0.030	12.323
46	462938	7512408	9	7.132	3.200	10.332	0.009	5.688
47	462939	7511911	20	5.002	9.192	14.194	0.019	7.814
48	467573	7516019	58	27.267	5.384	32.651	0.050	17.974
50	426000	7526000	10	3.084	4.540	7.624	-0.006	4.197
51	427000	7527246	7	0.664	2.980	3.644	-0.023	2.006
52	429001	7529253	2	0.915	4.320	5.235	-0.038	2.882
53	432547	7528386	3	1.628	5.396	7.024	-0.022	3.867
54	433195	7529321	10	3.076	4.048	7.124	-0.025	3.922
55	467568	7516516	80	63.447	17.104	80.551	0.089	44.343
56	471243	7529713	47	26.491	23.156	49.647	0.101	27.331
57	471244	7530710	118	99.806	10.184	109.990	0.115	60.549
58	470808	7543349	6	2.918	21.092	24.010	0.073	13.218
59	464000	7524000	94	22.744	15.584	38.328	0.062	21.100
61	474020	7518242	1	12.043	0.000	12.043	0.046	6.630
62	474997	7512250	47	24.957	7.956	32.913	0.028	18.119
63	470004	7508245	12	17.364	3.384	20.748	0.031	11.422
65	464698	7514305	47	43.378	15.072	58.450	0.057	32.176
66	435946	7525666	0	0.000	4.920	4.920	0.034	2.708
67	432822	7525656	3	0.892	5.400	6.292	-0.006	3.464
68	437181	7528225	0	0.000	6.100	6.100	0.005	3.358
69	436329	7527579	0	0.000	7.900	7.900	0.020	4.349
70	434816	7530241	9	6.150	8.092	14.242	-0.007	7.840
71	434816	7530741	4	0.350	7.896	8.246	-0.005	4.539
72	433171	7529911	4	0.517	9.400	9.917	-0.027	5.459
73	434257	7529284	8	0.850	10.140	10.990	-0.016	6.050
74	432349	7531761	2	0.393	5.880	6.273	-0.006	3.453
75	432849	7531761	9	0.826	7.040	7.866	-0.004	4.330
76	424634	7529829	4	1.092	3.480	4.572	-0.022	2.517
77	423134	7529829	4	0.737	7.840	8.577	-0.001	4.722
78	428314	7530631	12	2.610	11.360	13.970	-0.015	7.690
79	428814	7530631	1	0.515	6.080	6.595	-0.028	3.631
80	429500	7529253	6	0.874	7.760	8.634	-0.038	4.753
81	430013	7524999	0	0.000	7.440	7.440	-0.008	4.096
82	429513	7524999	2	0.401	3.384	3.785	-0.003	2.084
83	432822	7525156	1	0.112	3.384	3.496	-0.002	1.924

**APPENDIX AV:** Oven dry weight (Dr.wt.bio) as portioned by proportions of various carbon containing polymers in comparison to the obtained Serowe carbon conversion factor (0.43).

Sp Plot	Dr.wt.bio	Chemical Comp. of Wood			Carbon Content (%) in Polymers			Lab-results AvgC-Cnt(%)	Sp Plot
		Cellulose 43%	Lignin 25.50%	Hemicelluloses 31.50%	(C <sub>6</sub> H <sub>10</sub> O <sub>5</sub> ) <sub>1.7</sub>	(C <sub>9</sub> H <sub>10</sub> O <sub>3</sub> (OCH <sub>3</sub> ) <sub>0.9</sub> - (C <sub>5</sub> H <sub>8</sub> O <sub>4</sub> )	44%		
1	22.10	9.50	5.64	6.96	4.18	3.44	3.13	9.57	1
2	8.14	3.50	2.07	2.56	1.54	1.27	1.15	3.52	2
3	7.95	3.42	2.03	2.50	1.50	1.24	1.13	3.44	3
4	5.14	2.21	1.31	1.62	0.97	0.80	0.73	2.23	4
5	4.18	1.80	1.07	1.32	0.79	0.65	0.59	1.81	5
6	19.77	8.50	5.04	6.23	3.74	3.08	2.80	8.56	6
7	11.65	5.01	2.97	3.67	2.20	1.81	1.65	5.04	7
8	12.81	5.51	3.27	4.04	2.42	1.99	1.82	5.55	8
9	7.51	3.23	1.92	2.37	1.42	1.17	1.06	3.25	9
10	13.64	5.86	3.48	4.30	2.58	2.12	1.93	5.90	10
15	37.42	16.09	9.54	11.79	7.08	5.82	5.30	16.20	15
16	23.51	10.11	6.00	7.41	4.45	3.66	3.33	10.18	16
18	8.46	3.64	2.16	2.66	1.60	1.32	1.20	3.66	18
19	16.71	7.18	4.26	5.26	3.16	2.60	2.37	7.23	19
20	21.09	9.07	5.38	6.64	3.99	3.28	2.99	9.13	20
21	14.82	6.37	3.78	4.67	2.80	2.30	2.10	6.42	21
22	15.32	6.59	3.91	4.82	2.90	2.38	2.17	6.63	22
23	13.75	5.91	3.51	4.33	2.60	2.14	1.95	5.95	23
24	11.87	5.10	3.03	3.74	2.24	1.85	1.68	5.14	24
31	7.17	3.08	1.83	2.26	1.36	1.12	1.02	3.10	31
32	9.59	4.12	2.44	3.02	1.81	1.49	1.36	4.15	32
35	1.25	0.54	0.32	0.39	0.24	0.19	0.18	0.54	35
36	3.72	1.60	0.95	1.17	0.70	0.58	0.53	1.61	36
37	12.08	5.20	3.08	3.81	2.29	1.88	1.71	5.23	37
38	4.05	1.74	1.03	1.28	0.77	0.63	0.57	1.75	38
39	6.59	2.83	1.68	2.08	1.25	1.03	0.93	2.85	39
40	1.92	0.83	0.49	0.61	0.36	0.30	0.27	0.83	40
41	7.41	3.19	1.89	2.33	1.40	1.15	1.05	3.21	41
42	11.35	4.88	2.90	3.58	2.15	1.77	1.61	4.92	42
43	21.22	9.12	5.41	6.68	4.01	3.30	3.01	9.19	43
44	7.18	3.09	1.83	2.26	1.36	1.12	1.02	3.11	44
45	12.32	5.30	3.14	3.88	2.33	1.92	1.75	5.34	45
46	5.69	2.45	1.45	1.79	1.08	0.88	0.81	2.46	46
47	7.81	3.36	1.99	2.46	1.48	1.22	1.11	3.38	47
48	17.97	7.73	4.58	5.66	3.40	2.80	2.55	7.78	48
50	4.20	1.80	1.07	1.32	0.79	0.65	0.59	1.82	50
51	2.01	0.86	0.51	0.63	0.38	0.31	0.28	0.87	51
52	2.88	1.24	0.73	0.91	0.55	0.45	0.41	1.25	52
53	3.87	1.66	0.99	1.22	0.73	0.60	0.55	1.67	53
54	3.92	1.69	1.00	1.24	0.74	0.61	0.56	1.70	54
55	44.34	19.07	11.31	13.97	8.39	6.90	6.29	19.20	55
56	27.33	11.75	6.97	8.61	5.17	4.25	3.87	11.83	56
57	60.55	26.04	15.44	19.07	11.46	9.42	8.58	26.22	57
58	13.22	5.68	3.37	4.16	2.50	2.06	1.87	5.72	58
59	21.10	9.07	5.38	6.65	3.99	3.28	2.99	9.14	59
61	6.63	2.85	1.69	2.09	1.25	1.03	0.94	2.87	61

62	18.12	7.79	4.62	5.71	3.43	2.82	2.57	7.85	62
63	11.42	4.91	2.91	3.60	2.16	1.78	1.62	4.95	63
65	32.18	13.84	8.20	10.14	6.09	5.01	4.56	13.93	65
66	2.71	1.16	0.69	0.85	0.51	0.42	0.38	1.17	66
67	3.46	1.49	0.88	1.09	0.66	0.54	0.49	1.50	67
68	3.36	1.44	0.86	1.06	0.64	0.52	0.48	1.45	68
69	4.35	1.87	1.11	1.37	0.82	0.68	0.62	1.88	69
70	7.84	3.37	2.00	2.47	1.48	1.22	1.11	3.39	70
71	4.54	1.95	1.16	1.43	0.86	0.71	0.64	1.97	71
72	5.46	2.35	1.39	1.72	1.03	0.85	0.77	2.36	72
73	6.05	2.60	1.54	1.91	1.14	0.94	0.86	2.62	73
74	3.45	1.48	0.88	1.09	0.65	0.54	0.49	1.50	74
75	4.33	1.86	1.10	1.36	0.82	0.67	0.61	1.87	75
76	2.52	1.08	0.64	0.79	0.48	0.39	0.36	1.09	76
77	4.72	2.03	1.20	1.49	0.89	0.73	0.67	2.04	77
78	7.69	3.31	1.96	2.42	1.45	1.20	1.09	3.33	78
79	3.63	1.56	0.93	1.14	0.69	0.56	0.51	1.57	79
80	4.75	2.04	1.21	1.50	0.90	0.74	0.67	2.06	80
81	4.10	1.76	1.04	1.29	0.77	0.64	0.58	1.77	81
82	2.08	0.90	0.53	0.66	0.39	0.32	0.30	0.90	82
83	1.92	0.83	0.49	0.61	0.36	0.30	0.27	0.83	83

**APPENDIX BI:** The Fresh-Dry weight woody Biomass Ratio (*FDBR*) derived from Cyrille Kaboré (1991)'s MSc. thesis appendix *F* fresh and oven dry weights dataset on page 94.



**APPENDIX BII:** Vegetation Indices used as indicators for various biometric or biophysical quantities of vegetated surfaces. Copied and modified from (Davidson and Csillag, 2001). *NIR* and *R* correspond to the reflectances in the near-infrared and red wavelengths, respectively. “*a*” is the angle between the soil line and the *NIR* axis and “*g*” the slope of the soil line.

Index	Formula	Values Range	Sources
DVI	NIR-R	$\infty$	Richardson and Everitt (1992)
RVI	NIR/R	0 to $\infty$	Jordan (1969)
NDVI	$(NIR-R)/(NIR+R)$	-1 to +1	Rouse et al., (1973)
RDVI	$(NIR-R)/(\sqrt{NIR+R})$		Roujean and Breon (1995)
SAVI	$(NIR-R)(1+L)/(NIR+R+L)$ , where $L = 0.5$		Huete (1988)
MSAVI2	$2NIR+1 - \sqrt{(2NIR+1)^2 - 8(NIR-R)}/2$		Qi et al., (1994)
IPVI	$NIR/(NIR+R)$	0 to +1	Crippen (1990)
MSR	$\{(NIR/R)-1\}/\sqrt{\frac{NIR}{R}+1}$		Chen (1996)
PVI	$\sin(a)*NIR-\cos(a)*red$	-1 to +1	Richardson and Wiegand (1977)
WDVI	$NIR-g*red$	$\infty$	Clevers (1988)

**APPENDIX BIII:** Equations for the processing of images at high resolution-*Landsat-7 ETM+* data for the EBE.

1. Convert DN values back to radiances (at-satellite spectral radiances). This is accomplished with the equation:

$$L\lambda = L_{\min} + (L_{\max} - L_{\min})/255 * DN$$

Using map calc in Ilwis.  $L\lambda$  is the spectral radiance in  $Wm^{-2} sr^{-1} \mu m^{-1}$ , the DN is a DN map of s specific wavelength/band i.e. the raw data; or equation:

$$L\lambda_i = a + (b - a)/255 * DN$$

Where  $a = \text{Bias}$ ,  $(b - a) = \text{Gain}$  and  $DN = \text{digital numbers in band } i$ .  $L\lambda_i = mWcm^{-2} sr^{-1} \mu m^{-1}$ .

2. Compute the NDVI (best computed using spectral radiances than DNs), at-satellite NDVI using equation:

$$NDVI_{\text{toa}} = (L\lambda_i B4 - L\lambda_i B3)/(L\lambda_i B4 + L\lambda_i B3)$$

Using map calc in Ilwis. The Normalized Difference Vegetation Index (NDVI) is a measure of the amount and vigour of vegetation at the surface. The magnitude of NDVI is related to the level of photosynthetic activity in the observed vegetation. Generally, higher values of NDVI indicate greater vigour and amount of vegetation. (See AHAS for details).

3. The earth-sun distance ( $d$ ) in astronomical units (Iqbal, 1983) can be computed from this equation:

$$d = 1 + 0.0167 \sin\{2\pi(dy - 93.5)/365\}$$

Where  $dy$  = day in the year (1 to 365), and  $d$  is in AU (astronomical units). Alternatively, a spreadsheets known as the SunAngle is used to automatically compute  $d$ .

4. Calculation of the band-wise spectral reflectance at the top of the atmosphere (toa) is achieved by equation:

$$Rp(\lambda_i) = \pi L \lambda_i d^2 / k(\lambda_i) \cos\theta$$

Where  $k(\lambda_i)$  = spectral incoming solar radiation with  $k$  having  $mWcm^{-2}\mu m^{-1}$  as its unit,  $\theta$  = solar-zenith angle and  $Rp(\lambda_i)$  = albedo at toa. NB: the sun does not reflect in Band 6. Reflectance is a ratio or %.

The albedo is the ratio of the scattered radiation reflected at the top of the atmosphere to the incoming radiation reaching it, measured in the solar effective wavelength range of 0.3 and 3  $\mu m$  (visible). Satellites measure the spectral reflectance in narrow bands at the top of the atmosphere.

5. Calculation of the broadband reflectance at the top of the atmosphere (the Planetary albedo- $Rp_{bb}$ ) is:

$$Rp_{bb} = \sum Rp(\lambda_i) * k(\lambda_i) / \sum k(\lambda_i)$$

Broadband surface albedo is the hemispherical surface reflectance of short-wave radiation between wavelength of 0.3 and 3  $\mu m$ .

6. To calculate  $r_o$  (the surface albedo), we need to compute  $\tau$  (the transmittance of the atmosphere) using equation:

$$r_o = Rp - C7/\tau^2 \quad \text{where } \tau = K \downarrow_{\text{gnd}} / K \uparrow_{\text{toa}}, \text{ e.g. } 884 \text{ (station}$$

pyranometer measurement)/1128 (from the Sun-angle spreadsheets) = 0.78.

$$\therefore r_o = (Rp_{bb} - 0.083)/(0.78)^2$$

7. To convert Band 6 to temperature in radians (T), first convert B6's DN values to radiance. Assuming emissivity ( $\epsilon'$ ) = 1, with the inversion of Planck's law, the 'T' in Kelvin at-satellite temperature is:

$$T_{\text{radtoa}} = k_2 / \ln[(k_1/L\lambda_i) + 1]$$

8. Using the station point map data (table),  $e_s$ ,  $e_a$ ,  $\epsilon'_a$  and  $L \downarrow_{\text{inst}}$  are calculated as follows; i.e. in an effort to determine the instantaneous incoming long-wave radiation ( $L \downarrow_{\text{inst}}$ ):

- a).  $e_s$  (saturated water vapour pressure, i.e., the maximum amount of  $H_2O$  vapour the air can hold at temperature ( $T_a$ ) in degree Celsius is:

$$e_s = 0.6108 * \exp((17.27 * T_a) / (237.3 + T_a)) * 10 \text{ (mbars conversion to kPa).}$$

b). From the equation:  $RH = (e_a/e_s)*100$ , we can compute  $e_a$  after obtaining  $e_s$  from the previous equation as:

$$e_a = RH * e_s / 100$$

c).  $\epsilon'_a$  (emissivity of the air/atmosphere) can be calculated as:

$$\epsilon'_a = 1.24 * (e_a / T_a)^{1/7} \quad \text{where } T_a \text{ is in Kelvin scale.}$$

d). Hence, the  $L\downarrow_{inst}$  is found by:

$$L\downarrow_{inst} = \sigma * \epsilon'_a * T_a^4 \quad \text{where } \sigma \text{ is } 5.67 * 10^{-8} \text{ Wm}^{-2}\text{K}^4, \text{ and } T_a \text{ in (k).}$$

9. The Energy Balance Equation (EBE) in its simplest form is:

**Net Radiation (Rn) = soil heat flux (G) + sensible heat flux (H) + latent heat flux (LE).**

$$\lambda E = Rn - G - H$$

G can be determined by the NDVI, H under well watered conditions is zero, L which is also denoted by the Greek letter  $\lambda$  is a conversion factor to get E into mm.

The ratio between the latent heat flux by the summation of the sensible and latent heat fluxes is called “evaporative fraction”. This evaporative fraction ( $\Lambda$ ) is almost constant over the day and is a good indicator of the hydrological situation. Also EBE can be written as:

$$Rn = K\downarrow - K\uparrow + L\downarrow - L\uparrow$$

$$Rn = (1 - alb) * K\downarrow + L\downarrow - L\uparrow \quad \text{used in Ilwis map calc.}$$

When the albedo increases, the Rn reduces keeping the vegetation cooler. On the image, when the albedo is high, one can rightly assume that the area of interest is dry. Water from trees is released through the stomata. The radiometer is used to monitor the leaf surface area temperature ( $T_s$ ), which is usually close to the air temperature ( $T_a$ ), i.e.  $T_s \cong T_a$ ; here the NDVI is 0.7 on a well-watered crop. When the NDVI is 0.4, the vegetation tends to change the colour to a more reflective colour.

$$\text{Sensible heat flux (H)} = e_a C_p (T_s - T_a) / r_{ah}$$

Where  $e_a$  = air density ( $\text{kg/m}^3$ ),  $C_p$  = specific heat capacity of air ( $\text{Jkg}^{-1}\text{K}^{-1}$ ),  $T_s$  = soil temperature,  $T_a$  = air temperature, and  $r_{ah}$  = aerodynamic resistance to heat transport.

$$r_{ah} = e_a C_p (T_s - T_a) / H$$

$$r_{ah} = \text{kgm}^{-3} \text{Jkg}^{-1} \text{K}^{-1} \text{K} / \text{Js}^{-1} \text{m}^{-2}$$

$$r_{ah} = f(H)$$

$$\text{where } H = e_a C_p (T_s - T_a) / f(H)$$

as an implicitly equation in which one cannot make H the subject of the formula. This equation can only be solved by iteration. The iteration is stopped when the difference between  $|H_n - H_{n+1}| < 0.01$ . The above equation is solved pixel-by-pixel, 36 million times for Landsat. Aerodynamic resistance is also found by:

$$r_{ah} = 1/k^2 u [\ln(z/z_{om}) - \psi_m] * [\ln(z/z_{oh}) - \psi_h]$$

$$\psi_m = 2 * \ln\{(1 + \phi_m^{-1})/2\} + \ln\{(1 + \phi_m^{-2})/2 - 2 * \arctan \phi_m^{-1} + 0.5\pi\}$$

$$\phi_m = (1 - 16 * (z/L))^{-0.25}$$

$$L = - [(e_a C_p u_*^3 T_a) / kgH]$$

Now here at the start of the iteration, assume  $H = 0$  i.e. where its coolest coz of the presence of water, then  $L = -\infty$ ,  $\psi_m = 0$ ,  $\psi_h = 0$ , Assume:  $u_* = 1 \text{ m/s}$ ,  $e_a = 1 \text{ kg/m}^3$ ,  $C_p = 1000 \text{ J/kgK}$ ,  $T_s = 313 \text{ K}$ ,  $T_a = 293 \text{ K}$ ,  $g = 9.81 \text{ m/s}^2$ ,  $u_2 = 2 \text{ m/s}$ ,  $k = 0.41$ ,  $z = 100 \text{ m}$ ,  $z_{om} = 0.1$  and  $z_{oh} = 0.01$ .

How do you get the friction velocity ( $u_*$ )?

$$u/u_* = 1/k * [\ln(z/z_{om}) - \psi_m]$$

$$u_* = ku / \ln((z/z_{om}) - \psi_m)$$

#### 10. The Soil Heat Flux.

Flux is always calculated as a difference of potential, i.e.  $V_1 - V_2 / (R)$  resistance. Thus, the equation for soil heat flux used for experiments only or in local studies is:

$$G = \rho_s C_s (T_o - T_s) / r_s$$

In bare soil,  $G = 30\%$  of  $R_n$  while in forests,  $G$  is approximately zero. Estimating  $G$  from remote sensing (developed by Prof. Bastiaansen, 1995 and then further developed by various authors), for any pixel, the equation is:

$$G/R_n = (T_o * (0.32 * alb + 0.62 * alb^2)) * (1 - 0.98 * NDVI^4) / alb * 100$$

Where  $T_o$  = surface temperature of soil, alb in the numerator = surface albedo and alb in the denominator = average albedo.

However, the total amount of energy going into the soil during the day is equal to the amount of energy lost during the night. Therefore, soil heat flux is equal to zero and thus becomes negligible in the EBE.

11. The partitioning of the available energy ( $R_n - G$ ) between sensible and latent heat fluxes is governed by the availability of water. More water = more latent heat and less water = more sensible heat. Evaporation is variable during the day (24 hrs).

$$R_{n_{inst}} = H_{inst} + \lambda E_{inst} + G_{inst}$$

$$Rn_{inst} = (1 - alb)K\downarrow - \sigma\epsilon_0 T_o^4 - \sigma(1 - \epsilon_0)\epsilon' T_a^4 + \sigma\epsilon' T_a^4$$

The above equation is user friendly when you have the following parameters: alb; T<sub>o</sub>; T<sub>a</sub>; Rn; K<sub>↓</sub>; ε'; and ε<sub>o</sub>.

$$\lambda E_{inst} = Rn_{inst} - H_{inst} - G_{inst}$$

How to extrapolate from instantaneous to daily values? What else has to be measured in order to do so?

$$\Lambda_{inst} = LE/(LE + H) = LE/(Rn - G) = \Lambda_{day}$$

$$\Lambda_{inst} = LE_{inst}/(Rn_{inst} - G_{inst})$$

$$\Lambda_{inst} = \Lambda_{day}$$

where  $\Lambda_{inst}$  = evaporative fraction,  $LE/(LE + H)$  = constant during the day, this was observed and  $G \neq 0$  for the image but during the day it tends to zero and thus can be cancelled out in the following equation.

$$\Lambda_{day} = LE_{day}/(Rn_{day} - G_{day})$$

Evaporative fraction is a fraction that converts water into vapour. Thus, 0.2 evaporative fraction means 20% of the energy is used to convert water onto vapour.

$$E_{day} = Rn_{day} * \Lambda_{inst} / L \quad \text{where } Rn_{day} = (Wm^{-2})$$

Final equation is:  $E_{day} \text{ (mm/day)} = Rn_{day} * \Lambda_{inst} / 28.8$  where  $\Lambda_{inst}$  is from the image.

$$Rn_{day} = (1 - r_{oday})K\downarrow_{day} + L\downarrow_{day} - L\uparrow_{day} \quad \text{daily average values.}$$

$$L\downarrow_{day} = \sigma * \epsilon'_{average} * T_a^4 \quad T_a = \text{daily air temp average, } \epsilon'_{average} =$$

emissivity of the atmosphere and  $T_{oaverage}$  below as surface temperature average.

$$L\uparrow_{day} = \sigma * ((1 - \epsilon_0)\epsilon'_{average} * T_a^4 + \epsilon_0 * T_o^4)$$

$$\Delta L_{day} = -\sigma * ((T_{max}^4 + T_{min}^4)/2) * (0.34 - 0.14\sqrt{e_a}) * (1.35(K\downarrow/K\downarrow_{exoday}) - 0.35)$$

where  $e_a$  is KPa.

$$\Delta L_{day} = -110 * \tau_{day} \quad \text{use } \tau = 0.8$$

12. Objective: to calculate  $Rn_{inst}$  by hand;

$$Rn_{inst} = (1 - r_o)K\downarrow_{inst} + L\downarrow_{inst} - L\uparrow_{inst}$$

Where all the  $insts$  are maps and  $L\downarrow_{inst} = \sigma\epsilon'_a T_a^4$ .

$$\epsilon'_a = 1.24 * (e_a / T_{ainst})^{1/7}$$

where  $e_a$  is in mbars and  $T_{a_{inst}}$  in Kelvin and  $\epsilon'_a$  is the emissivity of the atmosphere.

$$RH = (e_a/e_s)*100$$

Where  $e_a$  = actual water vapour pressure,  $e_s$  = saturated water vapour pressure.

$$e_s \text{ (mbars)} = 0.6108*\exp((17.27*T_a)/(237.3 + T_a)) \quad T_a \text{ in } ^\circ\text{C, also } \times 10 \text{ to}$$

change 0.6108 KPa to mbars.

Determine the out-going long-wave radiation:

$$L\uparrow_{inst} = \sigma\epsilon_o T_o^4 + (1 - \epsilon_o)L\downarrow_{atm}$$

$T_o$  = surface temp at the ground,  $(1 - \epsilon_o)$  = reflection which is the same as formula  $(1 - \epsilon_o)*\sigma\epsilon'_a T_{a_{inst}}^4$ -already calculated.

$$\epsilon_o = \alpha + \beta*\ln(\text{NDVI})$$

where  $\alpha = 1.009$  and  $\beta = 0.047$ - can only be applied if the NDVI was computed as the NDVI at the ground using radiance values at the ground, i.e.,

$$\text{NDVI} = [(\text{radianceB4} - \text{radianceB3})/(\text{radianceB4} + \text{radianceB3})]$$

13. Second option to determine  $L\uparrow_{inst}$ :

a).  $L\uparrow_{toa}$  (Ilwis map) as seen by the satellite at the top of the atmosphere:

$$L\uparrow_{toa} = \sigma T_{rad}^4$$

$$L\uparrow_{gnd} = 1.05*L\uparrow_{toa} - 50.32 \quad \text{this should also be equal to } L\uparrow_{inst}.$$

To convert NDVI measured at-satellite to NDVI on the ground, this equation may be used:

$$\text{NDVI}_{toa} = \text{radB4} - \text{radB3}/\text{radB4} + \text{radB3}$$

$$\text{NDVI}_{gnd} = -0.043 + 1.008*\text{NDVI}_{toa}$$

$$\epsilon_{ognd} = 1.009 + 0.047*\ln(\text{NDVI}_{gnd})$$

Remember!!  $\text{Rad}_{bb} = \sigma*T_{bb}^4$

$$\text{Rad}_{rb} = \epsilon_o*\text{Rad}_{bb} = \epsilon_o\sigma T_{bb}^4 = \sigma T_{rb}^4$$

$$T_{rad} = \epsilon_o^{1/4}*T_k = \epsilon_o^{0.25}*T_k \text{ (steffan Boltzman)}$$

$\therefore T_o = T_{rad}/\epsilon_o^{0.25}$  where  $T_o$  = surface temp map.  
 $\text{Wm}^{-2} = 0.0864 \text{ MJm}^{-2} \text{ day}^{-1}$